This document is the Accepted Manuscript version of a Published Work that appeared in final form in Organic Electronics 20 (2015) 15–23 http://dx.doi.org/10.1016/j.orgel.2015.01.039

Indoline as Electron Donor Unit in "Push-Pull" Organic Small Molecules for Solution Processed Organic Solar Cells: Effect of the Molecular π-Bridge on Device Efficiency.

*Núria F. Montcada[1], Lydia Cabau[1], Challuri Vijay Kumar [1], Werther Cambarau[1] and Emilio Palomares[1,2]**

1. Foundation Institute of Chemical Research of Catalonia (ICIQ). Avda. Països Catalans, 16. Tarragona. E-43007. Spain.

2. Institució Catalana de Recerca I Estudis Avançats (ICREA). Passeig. Lluís Companys, 23. E-08010. Barcelona. Spain.

Graphical Abstract

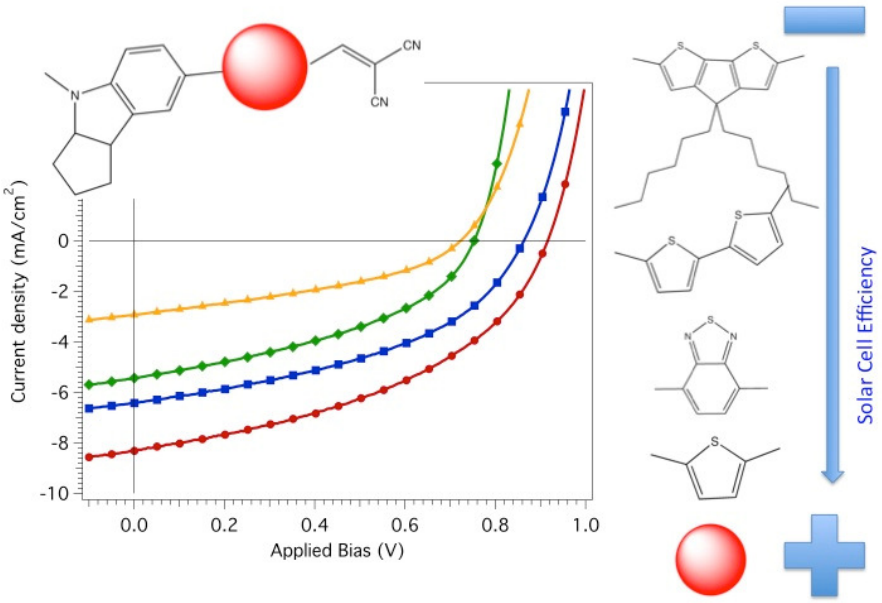

Highlights:

- Novel small molecules using indoline as electron donor for efficient organic solar cells
- The differences in efficiency can be explained by the differences in light harvesting and charge recombination.
- The pi-bridge results key to achieve high photocurrent and slow charge recombination kinetics.
- No clear correlation between charge mobility, film morphology and solar cell efficiency.

ABSTRACT

In this work we have synthesized and characterized four indoline-based small organic molecules for their use as electron donor moiety in bulk-heterojunction solution processed organic solar cells combined with $PC_{70}BM$ as electron acceptor. Our results show a wide range of light to energy efficiencies from 0.8 to 3.5% under standard measurement conditions. An initial analysis suggests that the main limitation is the device photocurrent due to the device film thickness. Yet, charge transfer dynamics were studied to correlate charge loss mechanisms to π-bridge structural variations and, moreover, mobility measurements were also carried out to fully explain these device limitations.

1. Introduction

Bulk-heterojunction organic solar cells (BHJ-OSC) have been intensively studied over the past decades [1-10]. In one hand, from the scientific point of view, organic solar cells still present many unsolved questions that drive the entire field, for example the processes involved in charge generation, charge recombination, energetic disorder and device loss mechanisms. On the other hand, the promise to obtain an efficient, non-toxic and cheaper technology for solar-to-energy conversion moves forward the search and design of new materials and device architectures.[11-16]

Current record efficiency, for single junction solution processed devices made using individual light absorber polymers, is close to 10%. Moreover, recent results in the use of small organic molecules instead of polymers in solution-processed devices have also demonstrated efficiencies as high as 8-9%[14, 17, 18] and the latest record efficiency reaching efficiencies close to 10% [19, 20], under standard measurement conditions. Yet, most reported standard efficiencies for semiconductor polymers are often between η=6-7%[21-23] and for small molecule based devices, between η=5-6%[24-27] using solution processed methods.

We present herein a complete study that starts with the synthesis of indoline based small molecules as electron donor moiety for organic solar cell (smOSC). Additionally, it analyses the device efficiency, charge recombination processes and mobility that limit the device performance.

The introduction of donor-π-acceptor dyes in OPV has been extensively studied in the past [28-31] and it has several advantages for their use in solar cells. First of all, the presence of a charge transfer band allows greater light harvesting of the sun spectra with molecular extinction coefficients as high as 100.000 M^{-1} cm^{-1}. Second, it is feasible to tune the molecule energy levels

and thus to obtain HOMO values as low as -5.22 eV that may lead to devices with high open circuit voltage, V_{oc}, a high LUMO level that facilitates the charge dissociation at the donor/acceptor interface and, third the π-bridge molecular backbone conformation can be also tuned to determine the molecular optical absorption onset[23, 32, 33] and their semiconductor properties.

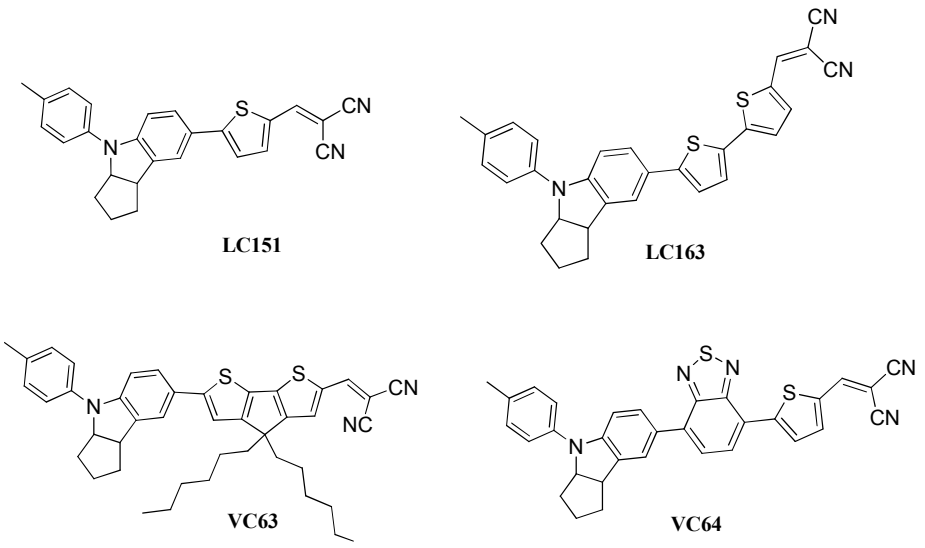

Scheme 1. Molecular structure of all indoline donor based small molecules **LC151**, **LC163**, **VC63** and **VC64**.

All molecules used in this study (**Scheme 1**) were synthesized using the indoline moiety as secondary electron donor unit due to its good donating ability and stability among other chemical groups, more frequently used donors such as triphenylamine. Indoline based molecules have been previously reported in both smOSC and Dye-Sensitized solar cells[34, 35]; however this kind of asymmetric structures are, in comparison, less explored in the smOPV field.[35-41] In order to make a more comprehensive study, all of these molecules were designed using the same donor (indoline) and acceptor moiety (dicyanovinyl); and, on the contrary, the π-bridge structure

was changed. We aim to compare and learn the effects in final device characteristics provided by the modification of the π-bridge of the **LC151** structure that will influence the charge mobility and the charge recombination dynamics; For example, inserting a new thiophene unit (**LC163**) promoting the intramolecular π-delocalization and also broadening the absorption range. We also replaced the thiophene π-bridge for a 4,4-dihexyl-4*H*-cyclopenta[1,2-*b*:5,4-*b'*]dithiophene moiety (**VC63**) to study the variation on light harvesting efficiency (LHE) of the molecule related to the presence of other conjugated system, which in turn, the presence of the pendant alkyl chains may improve the planarity of the molecule along film contributing in a more ordered aggregation and also favoring the π-delocalization.[42] The LHE is defined in **Equation 1**.

$$LHE(\lambda) = 1 - 10^{-\Gamma \sigma(\lambda)} \quad \textbf{(1)}$$

Where Γ is the number of moles of light absorber per unit area and σ is the absorption cross section in units area/mol obtained from the molecular extinction coefficient

Finally, a new strategy is proposed adding an auxiliary acceptor (benzothiadazole)[37, 38] between the donor and the π-bridge obtaining a D-A-π-A (**VC64**) architecture to further promote the intramolecular electron transfer and, thus, obtain a narrower band gap maintaining a deeper HOMO level, and, finally increase the stability due to a more effective electron dispersion from the indoline nitrogen units.[43] These results on the devices are analyzed further in this work.

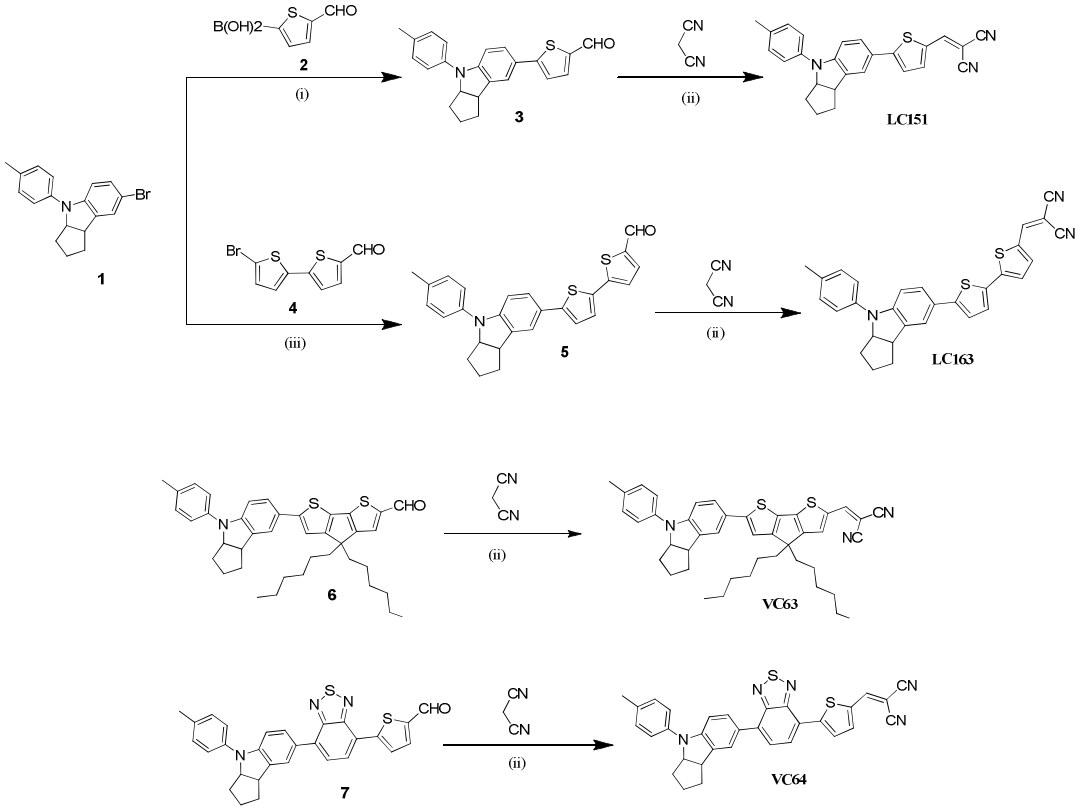

Scheme 2: Synthetic route of **LC** and **VC** molecules (*Reaction conditions:* (i) $Pd(PPh_3)_4$, 2 M K_2CO_3 aqueous solution, THF, 12 h, 80^0C; (ii) Malononitrile, β-alanine, dichloroethane, 12 h, reflux; (iii) n-BuLi, THF, $B(OCH_3)_3$, -78ºC, $Pd(PPh_3)_4$, 2 M K_2CO_3 aqueous solution, THF, 6 h 80 ºC.

2. Experimental

Materials

The following materials were used to synthesize all molecules: N,N-Dimethylformamide (DMF), phosphorytrichloride, 1,2dichloromethane, chloroform and THF were distilled before use. Pd(PPh3)4, N-bromosuccinimide (NBS), potassium carbonate, malononitrile, 4-tert-butylpyridine (TBP) and n-Butyllithium (2.0 M in hexane) were purchased from Sigma-Aldrich. For device fabrication: $PC_{70}BM$ was used as received from Solenne and Poly(3,4-

ethylenedioxythiophene):poly(styrenesulfonate) (PEDOT:PSS) from HC StarckBaytron P. Indium Tin Oxide (ITO) was purchased PSiOTec, Ltd., UK and blends were prepared in a Chloroform stock from Sigma-Aldrich.

Synthesis and characterization

The synthesis of **LC** and **VC** dyes are shown in the **scheme 2**. The intermediates 1[34], 3[43], 6[43] and 7[44] were prepared according to the literature.

Aldehyde precursors of final dyes were carried out using Suzuky coupling reacting the boronic acid of the π-bridge moiety and 7-bromo-4-(p-tolyl)-1,2,3,3a,4,8b-hexahydrocyclopenta[b]indole.

Knoevenagel condensation with malonitrile under basic conditions led to **LC151**, **LC163**, **VC63** and **VC64**.

For materials characterization. UV-Vis absorption spectra were measured in a 1 cm path-length quartz cell using a Shimadzu model 1700 spectrophotometer. Steady state fluorescence spectra were recorded using Spec model Fluoromax-3 spectrofluorometer using a 1 cm quartz cell. ^{1}H NMR spectra were recorded at 400MHz on a Bruker 400 Avance NMR spectrometer with X-WIN NMR software. ^{1}H NMR spectra were referenced to tetramethylsilane. ESI mass spectra were recorded on a Water Quattro micro (Water Inc., USA). Cyclic voltammetry experiments were carried out with a PC-controlled CH instruments model CHI620C electrochemical analyzer.

Synthesis of LC151. A solution of 5-(4-(p-tolyl)-1,2,3,3a,4,8b-hexahydrocyclopenta[b]indol-7-yl)thiophene-2-carbaldehyde(3)(100 mg, 0.27 mmol), malononitrile (55.18 mg, 0.83 mmol) and

β-alanine (1.48 mg, 0.016 mmol) in a mixture of 1.2 dichloroethane (10 mL) and ethanol (10 mL) was stirred under reflux overnight. The reaction mixture was cooled at room temperature; the precipitate was filtered off and washed thoroughly with ethanol providing the compound. ^{1}H-NMR (400 MHz, CDCl3) δ_H: 7.68 (s, 1H): 7.59 (d, J=4.2Hz, 1H), 7.37 (dd, J=8.3Hz, 2Hz, 2H), 7.25 (s, 1H), 7.16 (d, J=2Hz, 4H), 6.77(d, J=8.3Hz, 1H), 4.87 (m, 1H), 3.83 (m, 1H), 2.33 (s, 3H): 2.08 (m, 1H), 1.88 (m, 2H), 1.72 (m, 2H), 1.56 (m, 1H). 13C NMR (100 MHZ, CDCl3 ppm) δ: 159.07, 150.70, 150.01, 140.96, 138.91, 136.14, 133.23, 131.79, 130.02, 127.12, 123.18, 121.98, 121.83, 121.43, 115.05, 114.18, 107.14, 76.75, 69.71, 44.98, 35.33, 33.34, 24.31, 20.89. MS-ESI (m/z): [M] calculated for C30H23N3S2: 407.1459, found: 407.1451. (^{1}H-NMR/^{13}C NMR and HRMS spectra are shown in the ESI).

Synthesis of 5'-(4-(p-tolyl)-1,2,3,3a,4,8b-hexahydrocyclopenta[b]indol-7-yl)-[2,2'-bithiophene]-5-carbaldehyde(5). 7-bromo-4-(*p*-tolyl)-1,2,3,3a,4,8b-hexahydrocyclopenta[*b*]indole (**1)** (0.30 g, 0.917 mmol) was added to a round flask with 30 mL of THF and was stirred under nitrogen atmosphere at -78 ºC. ^{n}BuLi 2 M in hexane (0.41 mL, 1.08 mmol) was added and the mixture was stirred for 15 minutes at -78 ºC. After that, $B(OMe)_3$ (0.15 mL, 1.375 mmol) was added and the reaction was stirred overnight at -78 ºC. The crude (**1**) was warmed at room temperature. In another Schlenk, $Pd(PPh_3)_4$ (0.094 g, 0.025 mmol), 5'-bromo-[2,2'-bithiophene]-5-carbaldehyde (0.225 g, 0.82 mmol), K_2CO_3 2M (3.8 mL), 5'-bromo-[2,2'-bithiophene]-5-carbaldehyde (**4)** and THF (20mL) was added and the reaction was stirred at 70 ºC for 7 hours. Then water was added. The crude was extracted into $CHCl_3$, and the organic layer was dried over $NaSO_4$. The residue was purified by column chromatography (Hexane/Ethyl acetate 9.5:0.5) to obtain a red solid (0.220 g, 55% yield).

^{1}H-NMR (400 MHz, $CDCl_3$) δ_H: 9.82 (s, 1H), 7.64 (d, J=3.9Hz, 1H), 7.33 (s, 1H), 7.27 (dd, J=8.4Hz, 3.9Hz, 2H), 7.19 (d, J=3.9Hz, 1H) 7.16 (m, 4H), 7.09 (d, J=3.9Hz, 1H) 6.84 (d, J=8.4Hz, 1H), 4.81 (m, 1H), 3.83 (m, 1H), 2.32 (s, 3H), 2.04 (m, 1H), 1.90 (m, 2H), 1.77(m, 1H) 1.66 (m, 1H), 1.56 (m,1H). ^{13}C NMR (100 MHz, $CDCl_3$) δ: 182.56, 148.90, 148.73, 148.18, 148.05, 141.04, 140.14, 137.77, 135.95, 132.19, 130.07, 127.51, 125.72, 123.50, 122.54, 121.99, 120.65, 107.64, 69.55, 45.49, 35.35, 33.87, 24.63, 21.03. MS-ESI (*m/z*): $[M + Na]^+$ calculated for $C_{27}H_{23}NOS_2Na$: 464.1113, found: 464.1108. (^{1}H-NMR/^{13}C NMR and HRMS spectra are shown in the ESI).

Synthesis of LC163. A solution of **5** (180 mg, 0.41 mmol), malononitrile (81.14, 1.22 mmol) and β-alanine (2.19 mg, 0.024 mmol) in a mixture of dichloroethane (15 mL) and ethanol (15 mL) was stirred under reflux overnight. The reaction mixture was cooled at room temperature; the precipitate was filtered off and washed thoroughly with ethanol providing the compound.

^{1}H-NMR (400 MHz, $CDCl_3$) δ_H: 7.70 (s, 1H): 7.59 (d, J=4.3Hz, 1H), 7.36 (d, J=4.0Hz, 1H), 7.33 (s, 1H), 7.28 (dd, J=8.3Hz, 2Hz, 1H), 7.21 (d, J=4.3Hz, 1H), 7.16 (m, 4H), 7.12(d, J=4.0Hz, 1H), 6.82(d, J=8.3Hz), 4.82 (m, 1H), 3.83 (m, 1H), 2.32 (s, 3H): 2.06 (m, 1H), 1.89 (m, 2H), 1.77 (m, 2H), 1.67 (m, 2H). ^{13}C NMR (100 MHz, $CDCl_3$) δ: 150.38, 149.83, 149.57, 148.93, 140.36, 139.69, 135.83, 132.64, 132.25, 131.59, 129.89, 128.66, 125.71, 123.59, 123.23, 122.37, 122.13, 120.65, 113.75, 107.36, 69.41, 45.22, 35.16, 33.59, 29.70, 24.40, 20.83. MS-ESI (*m/z*): [M] calculated for $C_{30}H_{23}N_3S_2$: 489.1328, found: 489.1321. (^{1}H-NMR/^{13}C NMR and HRMS spectra are shown in the ESI).

Synthesis of VC63. A solution of **6** (80 mg, 0.13 mmol), malononitrile (35 mg, 0.38 mmol) and β-alanine (1 mg, 0.007 mmol) in a mixture of dichloroethane (6 mL) and ethanol (6 mL) was stirred under reflux overnight. The reaction mixture was cooled at room temperature; the precipitate was filtered off and washed thoroughly with ethanol providing the compound. ^{1}H-NMR (400 MHz, $CDCl_3$) δ_H: 7.64 (s, 1H), 7.45 (s, 1H), 7.36 (s, 1H), 7.31 (dd, J=8.3Hz, 2Hz, 1H), 7.16 (s, 4H), 7.04 (s, 1H), 6.83 (d, J=8.3Hz, 1H), 4.83 (m, 1H), 3.84 (m, 1H), 2.33 (s, 3H), 2.07 (m, 1H), 1.88 (m, 7H), 1.68 (m, 2H), 1.18 (m, 16H), 0.80 (t, J=6.8Hz, 6H), ^{13}C NMR (100 MHz, $CDCl_3$) δ: 166.12, 154.40, 152.89, 149.72, 148.98, 139.64, 135.92, 134.70, 132.32, 132.07, 129.90, 125.69, 124.11, 122.23, 120.65, 115.71, 115.26, 115.12, 107.45, 69.71, 69.44, 54.12, 45.21, 37.84, 35.21, 33.58, 31.55, 29.57, 24.52, 24.38, 22.59, 20.84, 14.00. MS-ESI (*m/z*): $[M + Na]^+$ calculated for $C_{43}H_{47}N_3NaS_2$: 692.3104, found: 692.3104. (^{1}H-NMR/^{13}C NMR and HRMS spectra are shown in the ESI).

Synthesis of VC64. A solution of **7** (120 mg, 0.24 mmol), malononitrile (48 mg, 0.73 mmol) and β-alanine (1.29 mg, 0.014 mmol) in a mixture of dichloroethane (10 mL) and ethanol (10 mL) was stirred under reflux overnight. The reaction mixture was cooled at room temperature; the precipitate was filtered off and washed thoroughly with ethanol providing the compound.

^{1}H-NMR (400 MHz, $CDCl_3$) δ_H: 8.23 (d, J=4.3Hz, 1H), 8.06 (d, J=7.7Hz, 1H), 7.85 (d, J=4.3Hz, 1H), 7.82 (m, 2H), 7.76 (dd, J=8.3Hz, 2Hz, 1H), 7.71 (d, J=7.7Hz, 1H), 7.18 (m, 3H), 6.99 (d, J=8.3Hz, 1H), 4.88 (m, 1H), 3.94 (m, 1H), 2.34 (s, 3H), 2.09 (m, 1H), 1.94 (m, 2H), 1.81 (m, 1H), 1.62 (m, 2H). ^{13}C NMR (126 MHz, $CDCl_3$) δ: 152.70, 151.70, 150.37, 149.31, 139.73, 139.15, 136.41, 135.59, 135.01, 132.26, 129.89, 129.41, 128.39, 127.78, 126.33, 125.70, 125.40,

122.13, 120.75, 114.38, 113.57, 107.36, 69.45, 45.37, 35.29, 33.62, 29.71, 24.43, 20.86. MS-ESI (*m/z*): $[M + Na]^+$ calculated for $C_{32}H_{23}N_5NaS_2$: 564.1287, found: 564.1277 (^{1}H-NMR/^{13}C NMR and HRMS spectra are shown in the ESI).

Device fabrication and characterization

Pre-patterned Indium Tin Oxide (ITO) 5 Ohm/square sodalime glass substrates were first rinsed with acetone to remove the residual photoresist layer. The substrates were then placed in a teflon holder and sequentially sonicated in acetone (1 × 10 min) and isopropanol (2 × 10 min), and finally dried under a nitrogen flow. The ITO substrates where ozone-treated in a UV-ozone cleaner for 30 min in ambient atmosphere, and subsequently coated in air with a layer of filtered (0.45 μm, cellulose acetate) solution of Poly(3,4-ethylenedioxythiophene):poly(styrenesulfonate) (4500 rpm 30 seconds followed by 3500 rpm 30 seconds). The PEDOT:PSS film was dried at 120 ºC under inert atmosphere for 15 min. Active layers were spin-coated (8000 rpm) in air over the PEDOT:PSS layer from a 20 mg/mL (total concentration) solution of donor derivative and $PC_{70}BM$ with a ratio 1:2 in weight. The solvent annealing step was carried out straight after deposition of the active layer by exposing the films to a saturated vapor atmosphere of dichloromethane in a controlled volume closed vessel. The vessel (100 mL) was filled with 10 mL of CH_2Cl_2 and left sealed for 5 min prior to the SVA step to ensure the saturation of the atmosphere. The substrates were exposed to the solvent vapors from 30 seconds to several minutes by placing them in the solvent vessel. [45]

The cathode layer was deposited by thermal evaporation in an ultra high vacuum chamber ($1 \cdot 10^{-6}$ mbar). Metals were evaporated through a shadow mask leading to devices with an area of 9 mm^2.

LiF (0.6 nm) and Al (80 nm) were deposited at a rate of 0.1 Å/s and 0.5-1 Å/s respectively. In the case of hole only and electron only devices the solar cells were prepared as explain above but for hole only devices the structure was ITO/PEDOT:PSS/donor:$PC_{70}BM$/Au and for electron only devices the structure was ITO/ZnOnp/donor:$PC_{70}BM$/Al. Regarding to the ZnO nanoparticles (np) the uniform layer (~ 35 nm) was deposited also by spin coating (2000 rpm) from a 10 mg/mL solution in isopropanol. All device efficiencies values correspond to masked devices with an active area of $9mm^2$.

For device characterization. The UV-Vis absorption spectra of films were measured using a Shimadzu UV-1700 spectrophotometer. The *I-V* characteristics of the devices were measured using a Sun 2000 Solar Simulator (150 W, ABET Technologies). The illumination intensity was measured to be 100 mW cm^{-2} with a calibrated silicon photodiode (NREL). The appropriate filters were utilized to faithfully simulate the AM 1.5G spectrum. The applied potential and cell current were measured with a Keithley 2400 digital source meter. The current to voltage (IV curve) was plotted automatically with a home-built Labview© software. The thickness of the films was measured with a stylus profilometer Ambios Tech. XP-1, from a scratch made in the middle of the film.

Results and discussion

The most relevant characterization parameters of all pristine molecules used in this study and its corresponding absorption, fluorescence spectra, as well as, the electrochemical data are listed in **Table 1**.

Table 1. UV-Visible, steady-state fluorescence and electrochemical data for **LC151**, **LC163**, **VC64** and **VC63** in solution.

Molecule	λ_{abs}*(nm)	λ_{em}*(nm)	E_{ox}**(V *vs.* Fc/Fc^{+})	$E_{0\text{-}0}$ (eV)	E_{HOMO} (eV)	E_{LUMO} (eV)
LC151	540 (43720)	670	0.34	2.09	-5.22	-3.13
LC163	561 (45568)	763	0.23	1.88	-5.11	-3.22
VC63	580 (26506)	725	0.13	1.90	-5.01	-3.11
VC64	572 (66666)	771	0.30	1.89	-5.18	-3.29

E_{ox}=Oxidation potential; $E_{0\text{-}0}$=Energy for the energy transition between the lowest vibrational ground state and the lowest vibrational excited state; E_{HOMO}=Highest Occupied Molecular Orbital and E_{LUMO}=Lowest Unoccupied Molecular Orbital. *Absorbance and emission spectra were measured in dichloromethane; In parenthesis, the molar extinction coefficient at λ_{abs} (in M^{-1} cm^{-1}). **The oxidation potential was measured in 0.1 M tetrabutylammonium hexafluorophosphate in dichloromethane at scan rate of 10 mV s^{-1}.

After the introduction of the fullerene, all blends were deposited over a substrate obtaining a 70 nm thick film from optimized conditions (see ESI). The Light Harvesting Efficiency (LHE) of **LC/PC_{70}BM** and **VC/PC_{70}BM** films were measured and shown in **Figure 1**.

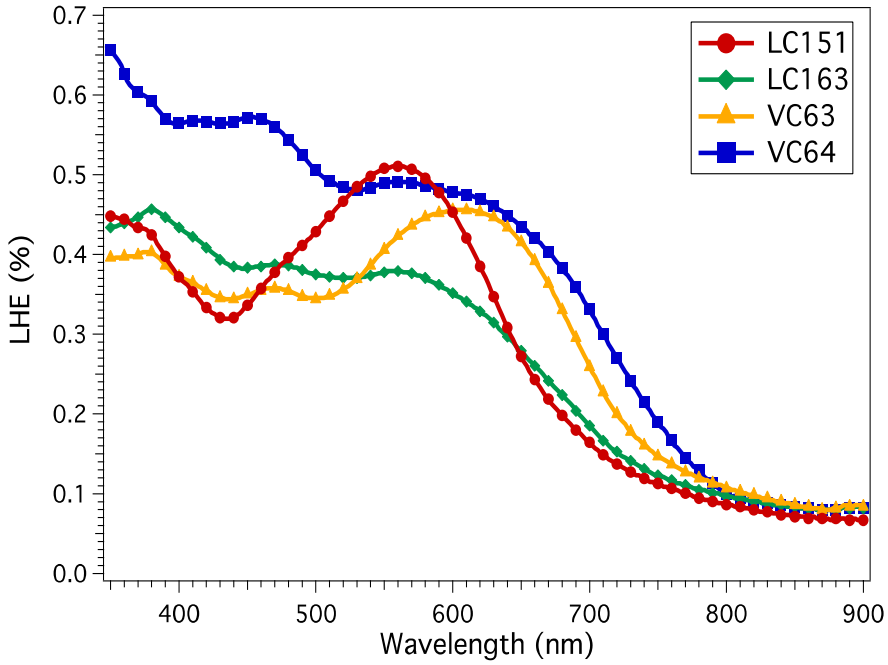

Figure 1. Light Harvesting Efficiencies (LHE) for a 70 nm thick film for optimized **LC151, LC163, VC63** and **VC64/$PC_{70}BM$** blends.

As can be seen in **Figure 1**, the maximum LHE shown corresponds to **LC151** and **VC64** molecules. The film thickness only allows a LHE of 57% in case of the **VC64**. Indeed thicker films will enhance LHE to greater values close to 100% but compromises the charge mobility as is described later on this work. Moreover, the comparison of the spectra give us the first evidences that a stronger π-delocalization promoted by the cyclopentadithiophene (**VC63**) and the benzothiadazole (**VC64**) increase the donor capability of the indoline; In both cases the absorption spectra is shifted to a longer wavelengths.

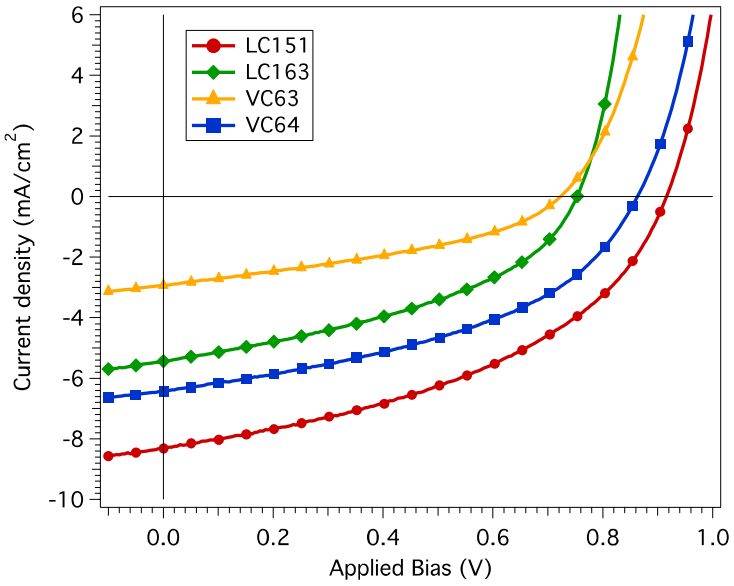

Figure 2. Measured current density *versus* voltage (*IV*) curves for optimized **LC151**, **LC163**, **VC63** and **VC64/PC$_{70}$BM** complete devices at 1 sun (100 mW cm^{-2}) conditions.

The **LC151/PC$_{70}$BM** devices resulted in the highest photocurrent efficiency (PCE), optimized devices were fabricated as described in the experimental section, with an optimized solvent vapor annealing (SVA) treatment of 120s. The obtained complete device of **LC151/PC$_{70}$BM** resulted in a PCE of 3.35% with a high V_{oc} of 915 mV and a J_{sc} of 8.3 mA cm^{-2} under standard measurement conditions, as shown in the current-voltage curve (**Figure 2**). In case of **LC163** a prominent decrease of the PCE occurs, and the same with all the performance parameters, with a reduction of the V_{oc} due to a shallower HOMO level. In **VC63**, similar to **LC163**, the PCE drastically decrease reaching values below 1%, and also the FF. **VC64** then, is placed as the second best molecule for its use in this kind of devices; however it should be take into account that even the LUMO level becomes closer to fullerene's and the photocurrent should be

promoted, the final J_{sc} is lower than **LC151**, probably due to nanomorphology (AFM images are shown in ESI) and, consequently, recombination dynamics variations.

Table 2. Performance parameters of optimized devices of **LC151**, **LC163**, **VC63** and **VC64/PC_{70}BM** fabricated under same conditions and same thickness (~70 nm). The values were obtained under sun-simulated (AM 1.5G) 100 mW cm^{-2} light irradiation.

Molecule	J_{sc} ($mAcm^{-2}$)	V_{oc} (mV)	FF (%)	PCE (%)
LC151	8.33	915	43.79	3.34
LC163	5.44	753	41.88	1.72
VC63	3.05	729	38.33	0.85
VC64	6.42	809	49.98	2.45

J_{sc} = Short-circuit current density; V_{oc} = Open-circuit voltage; FF = Fill factor; PCE = Photocurrent device efficiency.

Complementarily, the measured Incident Photon-to-Current Efficiency (IPCE) depicted in **Figure 3** shows broad spectra along the UV-Vis region, especially for **LC163**, **VC63** and **VC64** that shift to the red as the number of sulfur units increase as happened in the LHE measurements. It is important to notice that all the attempts to improve the intramolecular charge transfer noticeably decrease the photon conversion efficiency, probably due to the increase of the dipole moments that disfavor the mobility.[46] On the other hand, all the calculated J_{sc} from the IPCE spectra are in perfect agreement with the measured J_{sc} from *I-V* curves.

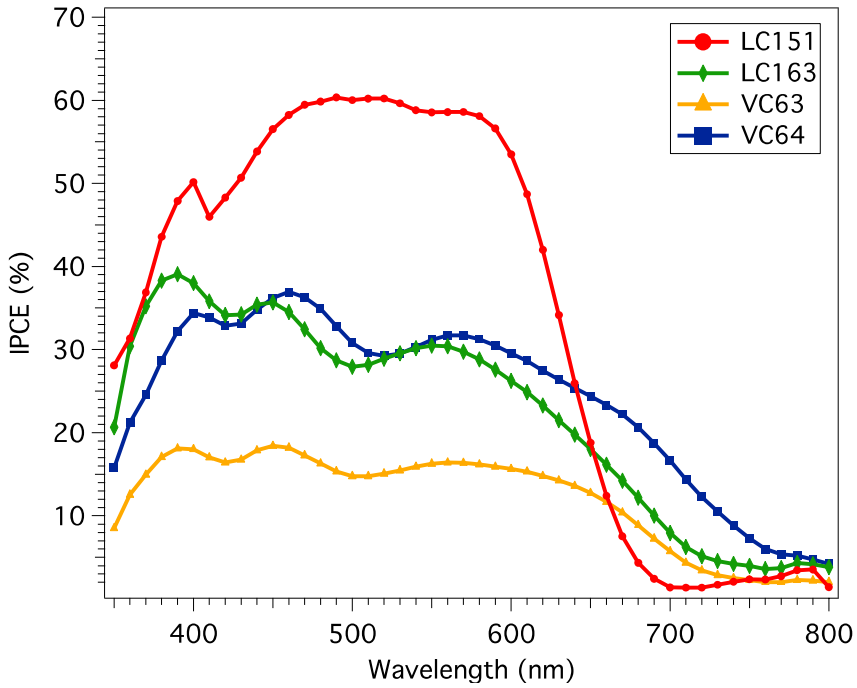

Figure 3. Incident photon-to-current efficiency of **LC151**, **LC163**, **VC63** and **VC64** complete devices.

The charge density and charge lifetime for these devices were measured using **Charge Extraction (CE)** and **Transient Photovoltage (TPV)** measurements respectively using same experimental set-up as reported before.[47-49] These measurements will serve us to understand some key limitations of these devices under operation conditions.

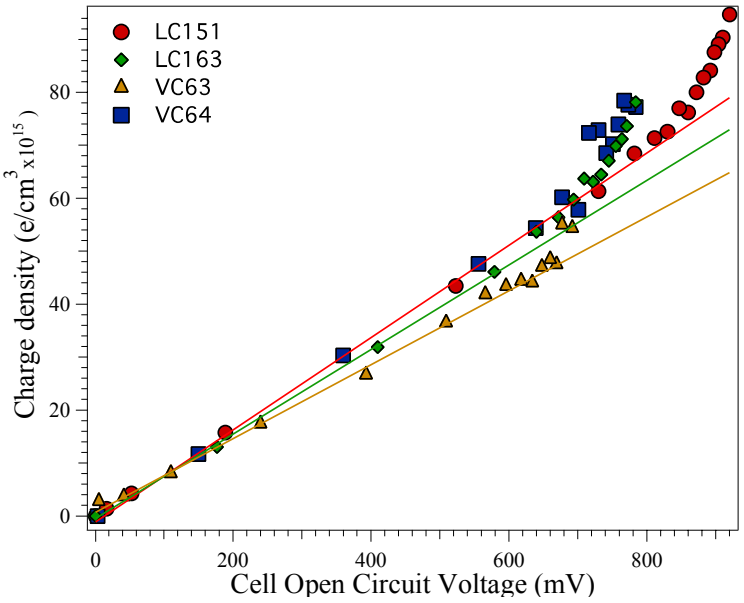

Figure 4. Measured extracted charges at different light induced device open circuit voltage of **LC151, LC163, VC63** and **VC64** smOSC.

As can be seen in **Figure 4,** the charge extraction follows a linear trend from 0 V (no illumination) to values close to illumination intensities approaching 1 sun that correspond to the maximum V_{oc} observed for each solar cell, and from that value until the measured maximum V_{oc} the exponential distribution appears, indicating that the charge storage capability of the bulk-heterojunction thin film is only given at a narrow range very close to 1 sun illumination and where the non-geminate recombination could be considered the most remarkable charge loss mechanism.[47, 50] In contrast, the linear correlation between the measured charge and the observed voltage corresponds to the geometrical capacitance, hence, at this point the device works as a capacitor and the charges are stored at the electrodes interface creating a noticeable electric field as is usually observed in very thin film devices.[51]

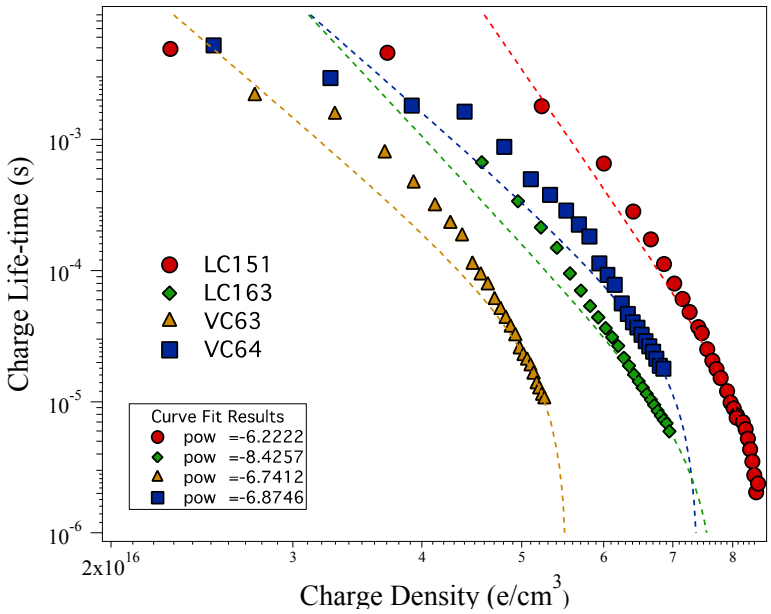

Figure 5. Charge life-time (ex: 570 nm) at different corresponding charge densities of **LC151, LC163, VC63** and **VC64** smOSC.

The data for the charge lifetime for all different solar cells at given charge density (from the CE measurements) is shown in **Figure 5**. As can be seen, **LC151** device presents the slowest charge life-time, which is consequent with devices having higher V_{oc} and, in this particular case, higher overall efficiency. Slower recombination dynamics are also in favor to more efficient charge collection. If the free carriers (polarons) recombination kinetics are too fast the polarons will recombine during their transport to the electrodes and, hence, the devices will have much lower efficiencies. Nonetheless, this is only true if the charge mobility values for actual devices are comparable, otherwise, the relation between device efficiency and non-geminate recombination kinetics becomes in a higher degree of complexity.

In this work, the hole and electron mobility values were calculated from hole and electron only device *IV* curves, respectively. The devices are forced to work within the Space Charge Limited Current (SCLC) conditions reached at very large potentials as shown in **Figure 6**. For example, in the particular case of **LC151/PC$_{70}$BM** devices, SCLC is reached after 3 V where the curve under light and dark are superimposed, both SCLC curves are fitted to the Murgatroyd equation, a variation of the Mott-Gurney equation that includes a field-dependent factor (**Equation 2**)[52] where μ (cm^2 V^{-1} s^{-1}) is the mobility coefficient, d (cm) is the film thickness, V_{eff} (V) is the applied voltage, β ($cm^{1/2}$ $V^{1/2}$) is the Poole-Frenkle factor and ε ($\varepsilon_0\varepsilon_r \approx 3$) is the media permittivity.

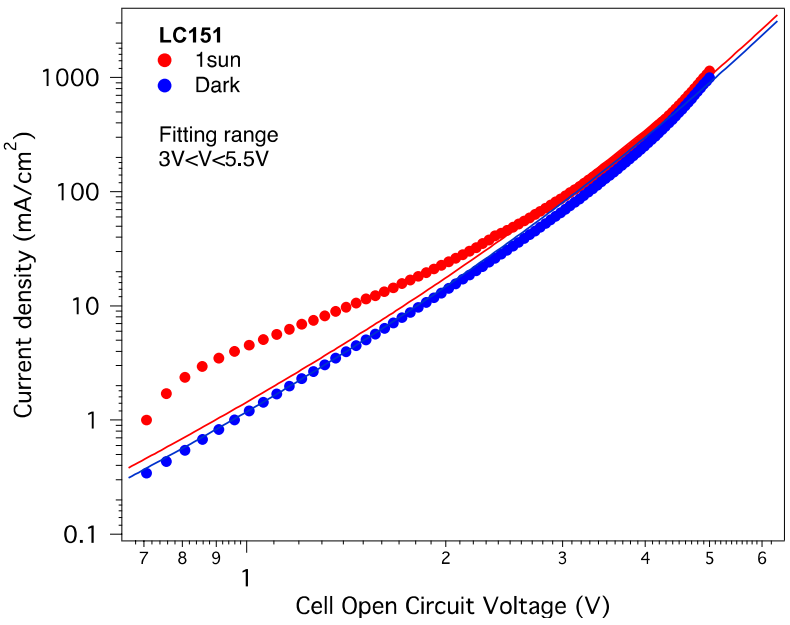

Figure 6. Current-voltage curves for a hole-only device of **LC151/PC$_{70}$BM** under sun-simulated irradiation (100 mW cm^{-2}) and in the dark. The fitting to Equation 1 is shown as a solid line.

$$J_{SCLC} = \frac{9}{8}\varepsilon\mu\frac{V_{eff}^2}{d^3}\exp\left(\frac{0.89\beta\sqrt{V_{eff}}}{\sqrt{d}}\right) \quad \textbf{(2)}$$

The corresponding hole mobility,μ_h, and the electron mobility,μ_e, for each type of solar cells are listed in **Table 3**.

Table 3. Hole and electron mobility data for **LC151**, **LC163**, **VC63** and **VC64** complete devices.

	h^+ mobility ($Vcm^{-2}s^{-1}$)	**e^- mobility ($Vcm^{-2}s^{-1}$)**
LC151	$2.0\pm0.8\cdot10^{-7}$	$2.8\pm0.8\cdot10^{-3}$
LC163	$1.0\pm0.2\cdot10^{-7}$	$4.6\pm0.4\cdot10^{-3}$
VC63	$2.3\pm1\cdot10^{-7}$	$4.6\pm1.5\cdot10^{-4}$
VC64	$4.5\pm2\cdot10^{-7}$	$4.9\pm1.4\cdot10^{-4}$

All the devices show a significant low hole mobility ($\mu=10^{-7}$ V cm^{-2} s^{-1}) when compared to other examples reported in the scientific literature for both, small molecules and low-bandgap polymers that usually display hole mobility values close to $\mu=10^{-4}$ V cm^{-2} s^{-1}.[53-55] Thus, the hole mobility values can be considered as one of the main limiting factors for these devices efficiency affecting the solar cell fill factor (FF)[56-58]. Yet, it is clear form our results that there are not a significant relationship between the low hole mobility data and the measured charge life-time. In addition, **VC63**/$PC_{70}BM$ and **VC64**/$PC_{70}BM$ blends present electron mobility values one order of magnitude lower than **LC151**/$PC_{70}BM$ and **LC163**/$PC_{70}BM$ indicating that the

formed nanostructure at the bulk-heterojunction disfavor the fullerene aggregation that serves as percolation pathway for electrons to the selective contact.

In conclusion we have designed and synthesized a series of novel indoline-based small molecules resulting in optimized device efficiencies close to 3.5% under standard measurement conditions. All optimized devices have light harvesting efficiencies below 60% limited by the thin thickness of the films obligated by the low mobility of the blend; indeed, one of the main limiting factors to the final J_{sc}. Moreover, the study of complete functional devices shows that active layers based on **LC151** present the highest efficiency mainly due to higher V_{oc} and J_{sc}. In the particular case of **VC64** the J_{sc} is further improved by the presence of the auxiliary acceptor (benzothiadazole moiety) as we assumed due to the proximity of LUMO energy levels of both donor and acceptor molecules, however the final value remains slightly below **LC151** probably because of some unfavorable nanomorphologies variances. The charge extraction measurements show similarities in electron densities at same voltages, and in addition all devices present similar geometric capacitance. Nevertheless, the TPV measurements show significant differences in the charge life-time, being the organic solar cells made using the **LC151** molecule the slowest in terms of charge recombination kinetics. Last but not least, the small molecules have hole mobility values 3 orders of magnitude lower than the best semiconductor polymers and other small organic molecules employed in organic solar cells. Indeed, this factor is also important and explains partially the observed low FF and limits the final solar cells efficiency. Particularly, for **VC63** and **VC64** the electron mobility values are also one order of magnitude slower suggesting a weak intermolecular interaction with fullerene mainly caused by the presence of the alkyl chains in case of **VC63** and smaller homo-aggregates of **VC64**. Based on the overall results presented herein we can conclude that for small organic molecules based on indoline as

secondary electron donor the mobility is the major issue to achieve efficiencies beyond 5% as the measured charges life-time using TPV show values in the order of more efficient organic solar cells made either using semiconductor polymers or small organic molecules.

ASSOCIATED CONTENT

Supporting Information Available: Full characterization of the molecules including ^{1}H-NMR/^{13}C NMR, HRMS, UV-Visible, emission spectroscopies and Square Wave Voltammetry plots, Description of device optimization and hole only and electron only device J-V curves at SCL.

AUTHOR INFORMATION

Corresponding Author

*To whom the correspondence should be addressed.

Prof. Emilio Palomares email: epalomares@iciq.es

Author Contributions

The manuscript was written through contributions of all authors. The small organic molecules were synthesized by Lydia Cabau and Challuri Vijay Kumar and measured the optical and electrochemical properties. Device and thin film characterization were carried out at ICIQ by Núria F. Montcada and Werther Cambarau under supervision of Prof. Emilio Palomares. All authors have given approval to the final version of the manuscript.

ACKNOWLEDGMENTS

The authors would like to thank the Spanish MINECO for financial support (projects CTQ-2010-18859 and CTQ-2013-47183R) and the Severo Ochoa Excellence Accreditation 2014-2018 (SEV-2013-0319). EP also thanks the ERC for the PolyDot funded project and the Catalan government for the 2009 SGR-207 project.

REFERENCES

[1] *A. Moliton*, *J.M. Nunzi*, How to Model the Behavior of Organic Photovoltaic Cells, Poly. Int., 55 (2006) 583-600.
[2] B.C. Thompson, J.M.J. Fréchet, Polymer-Fullerene Composite Solar Cells, Angew. Chem. Int. Ed., 47 (2008) 58-77.
[3] F.C. Krebs, Fabrication and Processing of Polymer Solar Cells: A Review of Printing and Coating Techniques, Sol. Energy Mater. Sol. Cells, 93 (2009) 394-412.
[4] T.M. Clarke, J.R. Durrant, Charge Photogeneration in Organic Solar Cells, Chem. Rev., 110 (2010) 6736-6767.
[5] J.D. Servaites, M.A. Ratner, T.J. Marks, Organic Solar Cells: A New Look at Traditional Models, Energy Environ. Sci., 4 (2011) 4410-4422.
[6] G. Li, R. Zhu, Y. Yang, Polymer Solar Cells, Nature Photonics, 6 (2012) 153-161.
[7] H.J. Snaith, How hould you measure your excitonic solar cells?, Energy Environ. Sci., 5 (2012) 6513-6520.
[8] Y. Lin, Y. Li, X. Zhan, Small Molecule Semiconductors for High-Efficiency Organic Photovoltaics, Chem. Soc. Rev., 41 (2012) 4245-4272.
[9] H.-L. Yip, A.K.-Y. Jen, Recent Advances in Solution-Processed Interfacial Materials for Efficient and Stable Polymer Solar Cells, Energy Environ. Sci., (2012).
[10] R.A.J. Janssen, J. Nelson, Factors Limiting Device Efficiency in Organic Photovoltaics, Adv. Mater., 25 (2013) 1847-1858.
[11] D. Credgington, R. Hamilton, P. Atienzar, J. Nelson, J.R. Durrant, Non-Geminate Recombination as the Primary Determinant of Open-Circuit Voltage in Polythiophene:Fullerene Blend Solar Cells: an Analysis of the Influence of Device Processing Conditions, Adv. Funct. Mater., 21 (2011) 2744-2753.
[12] C.M. Proctor, C. Kim, D. Neher, T.Q. Nguyen, Nongeminate Recombination and Charge Transport Limitations in Diketopyrrole-Based Solution Processed Small Molecule Solar Cells, Adv. Funct. Mater., 23 (2013) 3584-3594.
[13] Y. Lin, P. Cheng, Y. Liu, X. Zhao, D. Li, J. Tan, W. Hu, Y. Li, X. Zhan, Solution-Processable Small Molecules Based on Thieno[3,4-c]pyrrole-4,6-dione for High-Performance Solar Cells, Sol. Energy Mater. Sol. Cells, 99 (2012) 301-307.
[14] A.K.K. Kyaw, D.H. Wang, V. Gupta, J. Zhang, S. Chand, G.C. Bazan, A.J. Heeger, Efficient Solution-Processed Small-Molecule Solar Cells with Inverted Structure, Adv. Mater., 25 (2013) 2397-2402.

[15] J.Y. Oh, M. Shin, I.L. Lee, W.S. Jang, Y.-J. Lee, C.S. Kim, J.-W. Kang, J.-M. Myoung, H.K. Baik, U. Jeong, Highly Bendable Large-Area Printed Bulk Heterojunction Film Prepared by the Self-Seeded Growth of Poly(3-hexylthiophene) Nanofibrils, Macromolecules, 46 (2013) 3534-3543.
[16] Y. Li, L. Mao, Y. Gao, P. Zhang, C. Li, C. Ma, Y. Tu, Z. Cui, L. Chen, ITO-Free Photovoltaic Cell Utilizing a High-Resolution Silver Grid Current Collecting Layer, Sol. Energy Mater. Sol. Cells, 113 (2013) 85-89.
[17] J. Zhou, Y. Zuo, X. Wan, G. Long, Q. Zhang, W. Ni, Y. Liu, Z. Li, G. He, C. Li, B. Kan, M. Li, Y. Chen, Solution Processed and High Performance Organic Solar Cells Using Small Molecules with Benzodithiophenes Unit, J. Am. Chem. Soc., 135 (2013) 8484-8487.
[18] Y. Liu, C.-C. Chen, Z. Hong, J. Gao, Y.M. Yang, H. Zhou, L. Dou, G. li, Y. Yang, Solution-Processed Small-Molecule Solar Cells: Breaking the 10% Power Conversion Efficiency, Scientific Reports, 3 (2013) 3356.
[19] Q. Zhang, B. Kan, F. Liu, G. Long, X. Wan, X. Chen, Y. Zuo, W. Ni, H. Zhang, M. Li, Z. Hu, F. Huang, Y. Cao, Z. Liang, M. Zhang, T.P. Russell, Y. Chen, Small-molecule solar cells with efficiency over 9%, Nature Photon., (2014).
[20] B. Kan, Q. Zhang, M. Li, X. Wan, W. Ni, G. Long, Y. Wang, X. Yang, H. Feng, Y. Chen, Solution-Processed Organic Solar Cells Based on Dialkylthiol-Substituted Benzodithiophene Unit with Efficiency near 10%, J. Am. Chem. Soc., 136 (2014) 15529-15532.
[21] W. Li, K.H. Hendriks, W.S.C. Roelofs, Y. Kim, M.M. Wienk, R.A.J. Janssen, Efficient Small Bandgap Polymer Solar Cells with High Fill Factors for 300 nm Thick Films, Adv. Mater., 25 (2013) 3182-3186.
[22] L. Ye, S. Zhang, W. Ma, B. Fan, X. Guo, Y. Huang, H. Ade, J. Hou, From Binary to Ternary Solvent: Morphology Fine-tuning of D/A Blends in PDPP3T-based Polymer Solar Cells, Adv. Mater., 24 (2012) 6335-6341.
[23] B. Kim, X. Ma, C. Chen, Y. Ie, E.W. Coir, H. Hashemi, Y. Aso, P.F. Green, J. Kieffer, J. Kim, Energy Level Modulation of HOMO, LUMO, and Band-Gap in Conjugated Polymers for Organic Photovoltaic Applications, Adv. Funct. Mater., 23 (2013) 439-445.
[24] Y. Liu, X. Wan, F. Wang, J. Zhou, G. Long, J. Tian, Y. Chen, High-Performance Solar Cells using a Solution-Processed Small Molecule Containing Benzodithiophene Unit, Adv. Mater., 23 (2011) 5387-5391.
[25] J. Zhou, X. Wan, Y. Liu, G. Long, F. Wang, Z. Li, Y. Zuo, C. Li, Y. Chen, A Planar Small Molecule with Dithienosilole Core for High Efficiency Solution-Processed Organic Photovoltaic Cells, Chem. Mater., 23 (2011) 4666-4668.
[26] T.S. Van der Poll, J.A. Love, T.Q. Nguyen, G.C. Bazan, Non-Basic High-Performance Molecules for Solution-Processed Organic Solar Cells, Adv. Mater., 24 (2012) 3646-3649.
[27] C. Cui, J. Min, C.-L. Ho, T. Ameri, P. Yang, J. Zhao, C.J. Brabec, W.-Y. Wong, A New Two-Dimensional Oligothiophene End-Capped with Alkyl Cyanoacetate Groups for Highly Efficient Solution-Processed Organic Solar Cells, Chem. Comm., 49 (2013) 4409-4411.
[28] S.-W. Chiu, L.-Y. Lin, H.-W. Lin, Y.-H. Chen, Z.-Y. Huang, Y.-T. Lin, F. Lin, Y.-H. Liu, K.-T. Wong, A donor-acceptor-acceptor molecule for vacuum-processed organic solar cells with a power conversion efficiency of 6.4%, Chemical Communications, 48 (2012) 1857-1859.
[29] N.M. Kronenberg, M. Deppisch, F. Wurthner, H.W.A. Lademann, K. Deing, K. Meerholz, Bulk heterojunction organic solar cells based on merocyanine colorants, Chemical Communications, (2008) 6489-6491.

[30] N.M. Kronenberg, V. Steinmann, H. Bürckstümmer, J. Hwang, D. Hertel, F. Würthner, K. Meerholz, Direct Comparison of Highly Efficient Solution- and Vacuum-Processed Organic Solar Cells Based on Merocyanine Dyes, Advanced Materials, 22 (2010) 4193-4197.
[31] Y.-H. Chen, L.-Y. Lin, C.-W. Lu, F. Lin, Z.-Y. Huang, H.-W. Lin, P.-H. Wang, Y.-H. Liu, K.-T. Wong, J. Wen, D.J. Miller, S.B. Darling, Vacuum-Deposited Small-Molecule Organic Solar Cells with High Power Conversion Efficiencies by Judicious Molecular Design and Device Optimization, Journal of the American Chemical Society, 134 (2012) 13616-13623.
[32] B.W. D'Andrade, S. Datta, S.R. Forrest, P. Djurovich, E. Polikarpov, M.E. Thompson, Relationship Between the Ionization and Oxidation Potentials of Molecular Organic Semiconductors, Org. Electron., 6 (2005) 11-20.
[33] P.M. Beaujuge, J.M.J. Fréchet, Molecular Design and Ordering Effects in pi-Functional Materials for Transistor and Solar Cell Applications, J. Am. Chem. Soc., 133 (2011) 20009-20029.
[34] L. Cabau, L. Pallejà, J.N. Clifford, C.V. Kumar, E. Palomares, Light Soaking Effects on Charge Recombinationand Device Performance in Dye Sensitized Solar Cells Based on Indoline-Cyclopentadithiophene Chromophores, J. Mater. Chem. A, 1 (2013) 8994-9000.
[35] D. Demeter, V. Jeux, P. Leriche, P. Blanchard, Y. Olivier, J. Cornil, R. Po, J. Roncali, Tuning of the Photovoltaic Parameters of Molecular Donors by Covalent Bridging, Adv. Funct. Mater., (2013).
[36] H. Bürckstümmer, E.V. Tulyakova, M. Deppisch, M.R. Lenze, N.M. Kronenberg, M. Gsänger, M. Stolte, K. Meerholz, F. Würthner, Efficient Solution-Processed Bulk Heterojunction Solar Cells by Antiparallel Supramolecular Arrangement of Dipolar Donor–Acceptor Dyes, Angew. Chem. Int. Ed., 50 (2011) 11628-11632.
[37] L.-Y. Lin, Y.-H. Chen, Z.-Y.-. Huang, H.-W. Lin, S.-H. Chou, F. Lin, C.-W. Chen, Y.-H. Liu, K.-T. Wong, A Low-Energy-Gap Organic Dye for High-Performance Small-Molecule Organic Solar Cells, J Am Chem Soc, 133 (2011) 15822-15825.
[38] Y.-H. Chen, L.-Y. Lin, C.-W. Lu, F. Lin, Z.-Y. Huang, H.-W. Lin, P.-H. Wang, Y.-H. Liu, K.-T. Wong, J. Wen, D.J. Miller, S.B. Darling, Vacuum-Deposited Small-Molecule Organic Solar Cells with High Power Conversion Efficiencies by Judicious Molecular Design and Device Optimization, J. Am. Chem. Soc., 134 (2012) 13616-13623.
[39] G. Wei, X. Xiao, S. Wang, K. Sun, K.J. Bergemann, M.E. Thompson, S.R. Forrest, Functionalized Squaraine Donors for Nanocrystalline Organic Photovoltaics, ACS NANO, 6 (2012) 972-978.
[40] A.Y. Chang, Y.-H. Chen, H.-W. Lin, L.-Y. Lin, K.-T. Wong, R.D. Schaller, Charge Carrier Dynamics of Vapor-Deposited Small-Molecule/Fullerene Organic Solar Cells, Journal of the American Chemical Society, 135 (2013) 8790-8793.
[41] H.-I. Lu, C.-W. Lu, Y.-C. Lee, H.-W. Lin, L.-Y. Lin, F. Lin, J.-H. Chang, C.-I. Wu, K.-T. Wong, New Molecular Donors with Dithienopyrrole as the Electron-Donating Group for Efficient Small-Molecule Organic Solar Cells, Chem. Mater., 26 (2014) 4361-4367.
[42] Y.J. Kim, K.H. Park, J.-j. Ha, D.S. Chung, Y.-H. Kim, C.E. Park, The effect of branched versus linear alkyl side chains on the bulk heterojunction photovoltaic performance of small molecules containing both benzodithiophene and thienopyrroledione, Phys. Chem. Chem. Phys., 16 (2014) 19874-19883.
[43] W. Li, Y. Wu, Q. Zhang, H. Tian, W. Zhu, D-A-n-A Featured Sensitizers Bearing Phthalimide and Benzotriazole as Auxiliary Acceptor: Effect on Absorption and Charge

Recombination Dynamics in Dye-Sensitized Solar Cells, Appl. Mater. Interfaces, 4 (2012) 1822-1830.
[44] W. Zhu, Y. Wu, S. Wang, W. Li, X. Li, J. Chen, Z.-S. Wang, H. Tian, Organic D-A-n-A Solar Cell Sensitizers with Improved Stability and Spectral Response, Adv. Funct. Mater., 21 (2011) 756-763.
,[45] A. Viterisi, F. Gispert-Guirado, J.W. Ryan, E. Palomares, Formation of Highly Crystalline and Texturized Donor Domains in DPP(TBFu)2:PC71BM SM-BJH Devices via Solvent Vapour Annealing: Implications for Device Function, J. Mater. Chem., 22 (2012) 15175.
[46] H. Bürckstümmer, N.M. Kronenberg, M. Gsänger, M. Stolte, K. Meerholz, F. Würthner, Tailored merocyanine dyes for solution-processed BHJ solar cells, Journal of Materials Chemistry, 20 (2010) 240-243.
[47] A. Sánchez-Díaz, R. Pacios, U. Muñecas, T. T., E. Palomares, Charge Transfer Reactions in Near IR Absorbing Small Molecule Solution Processed Organic Bulk-Heterojunction Solar, Org. Electron., 12 (2011) 329-335.
[48] C.G. Shuttle, A. Maurano, R. Hamilton, B. O'Regan, J.C. de Mello, J.R. Durrant, Charge Extraction Analysis of Charge Carrier Densities in a Polythiophene/Fullerene Solar Cell: Analysis of the Origin of the Device Dark Current, Appl. Phys. Lett., 93 (2008) 183501.
[49] C.G. Shuttle, B. O'Regan, A.M. Ballantyne, J. Nelson, D.D.C. Bradley, A.J. Mello, J.R. Durrant, Experimental Determination of the Rate Law for Charge Carrier Decay in a Polythiophene: Fullerene Solar Cell, Appl. Phys. Lett., 92 (2008) 093311.
[50] A. Sánchez-Díaz, L. Burtone, M. Riede, E. Palomares, Measurements of Efficiency Losses in Blend and Bilayer-Type Zinc Phthalocyanine/C60 High-Vacuum-Processed Organic Solar Cells, J. Phys. Chem. C, 116 (2012) 16384-16390.
[51] D. Ray, L. Burtone, K. Leo, M. Riede, Detection of Trap Charge in Small Molecular Organic Bulk Heterojunction Solar Cells, Phys. Rev. B, 82 (2010) 125204.
[52] T. Kirchartz, Influence of Difussion on Space-Charge-Limited Current Measurements in Organic Semiconductors, Beilstein J. Nanotechnol, 4 (2013) 180-188.
[53] J. Zhou, X. Wan, Y. Liu, Y. Zuo, Z. Li, G. He, G. Long, W. Ni, C. Li, X. Su, Y. Chen, Small Molecules Based on Benzo[1,2-b:4,5-b']dithiophene Unit for High-Performance Solution-Processed Organic Solar Cells, J. Am. Chem. Soc., 134 (2012) 16345-16351.
[54] Y. Sun, G.C. Welch, W.L. Leong, C.J. Takacs, G.C. Bazan, A.J. Heeger, Solution-Processed Small-Molecule Solar Cells with 6.7% Efficiency, Nat. Mater., 11 (2012) 44-48.
[55] O.P. Lee, A.T. Yiu, P.M. Beaujuge, C.H. Woo, T.W. Holcombe, J.E. Millstone, J.D. Douglas, M.S. Chen, J.M.J. Fréchet, Efficient Small Molecule Bulk Heterojunction Solar Cells with High Fill Factors via Pyrene-Directed Molecular Self-Assembly, Adv. Mater., 23 (2011) 5359-5363.
[56] G.F.A. Dibb, F.C. Jamieson, A. Maurano, J. Nelson, J.R. Durrant, Limits on the Fill Factor in Organic Photoltaics: Distinguishing Nongeminative and Geminate Recombination Mechanisms, J. Phys. Chem. Lett., 4 (2013) 803-808.
[57] T. Kirchartz, T. Agostinelli, M. Campoy-Quiles, W. Gong, J. Nelson, Understanding the Thickness-Dependent Performance of Organic Bulk Heterojunction Solar Cells: The Influence of Mobility, Lifetime, and Space Charge, J. Phys. Chem. Lett., 3 (2012) 3470-3475.
[58] W. Tress, A. Petrich, M. Hummert, M. Hein, K. Leo, M. Riede, Imbalanced Mobilities Causing S-shaped IV Curves in Planar Heterojunction Organic Solar Cells, Appl. Phys. Lett., 98 (2011) 063301(063301-063303).

Supporting information

Indoline as Electron Donor Unit in "Push-Pull" Organic Small Molecules for Solution Processed Organic Solar Cells: Effect of the Molecular π-Bridge on Device Efficiency.

*Núria F. Montcada[1], Lydia Cabau[1], Challuri Vijay Kumar[1], Werther Cambarau[1] and Emilio Palomares[1,2]**

1. Foundation Institute of Chemical Research of Catalonia (ICIQ). Avda. Països Catalans, 16. Tarragona. E-43007. Spain.

2. Institució Catalana de Recerca I Estudis Avançats (ICREA). Passeig. Lluís Companys, 23. E-08010. Barcelona. Spain.

TABLE OF CONTENTS

S1. ^{1}H NMR, ^{13}C NMR and HRMS spectra

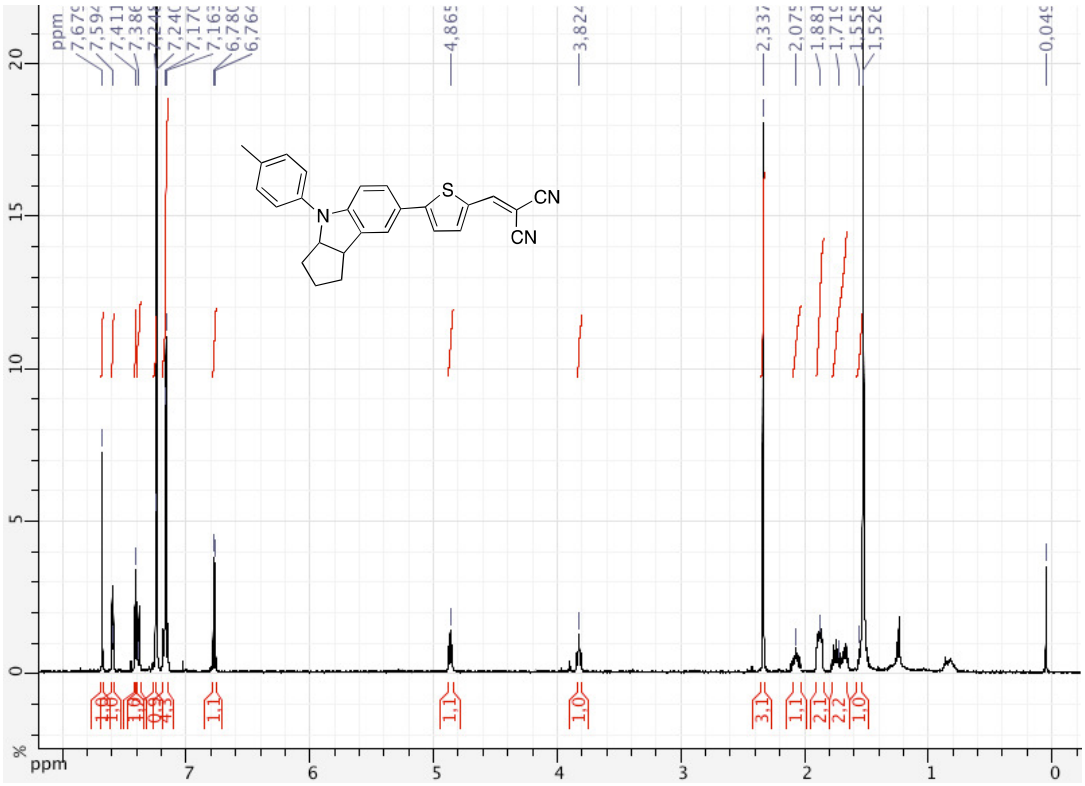

Fig. S1.1 ^{1}H NMR spectra of compound **LC151** recorded in $CDCl_3$.

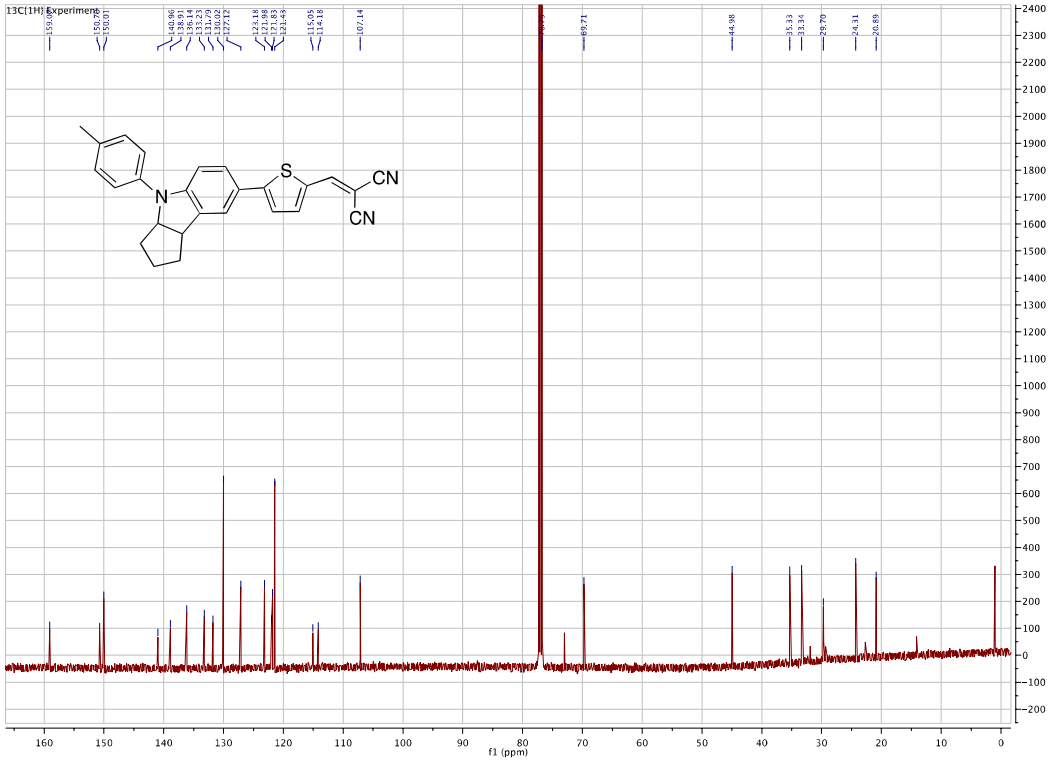

Fig. S1.2 ^{13}C NMR spectra of compound **LC151** recorded in $CDCl_3$.

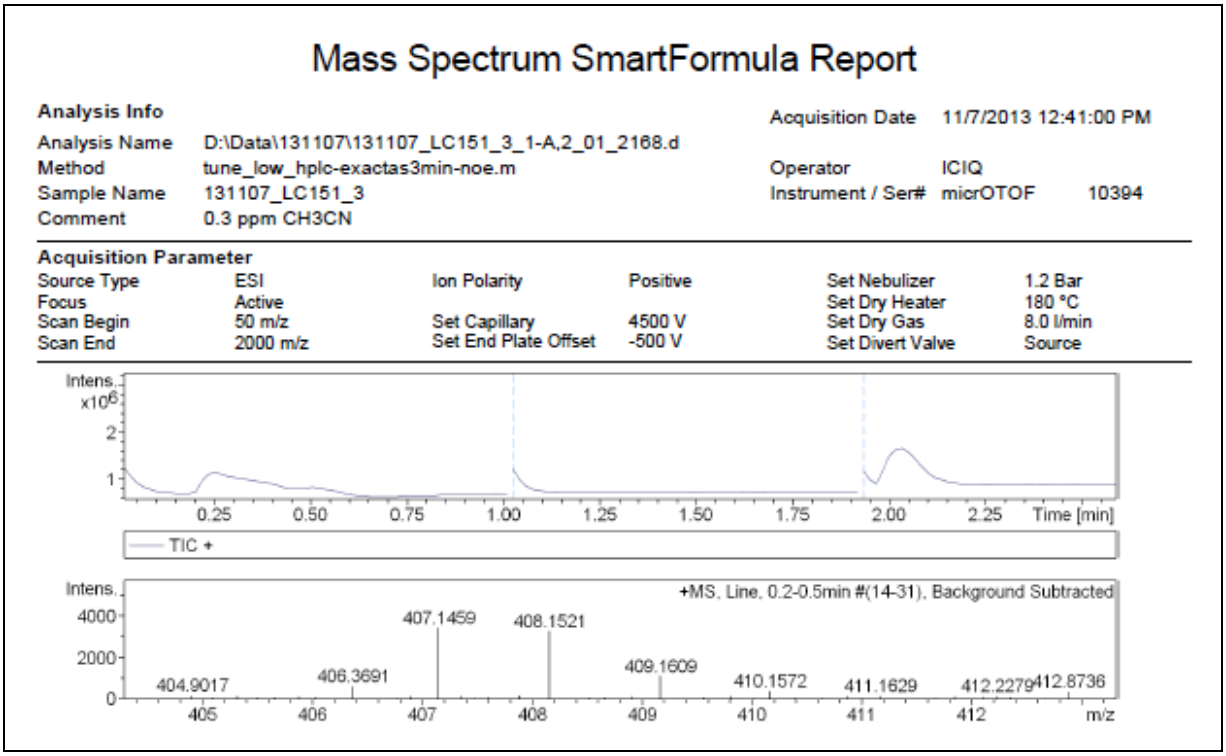

Fig. S1.3 HRMS (ESI) spectrum of compound **LC151**.

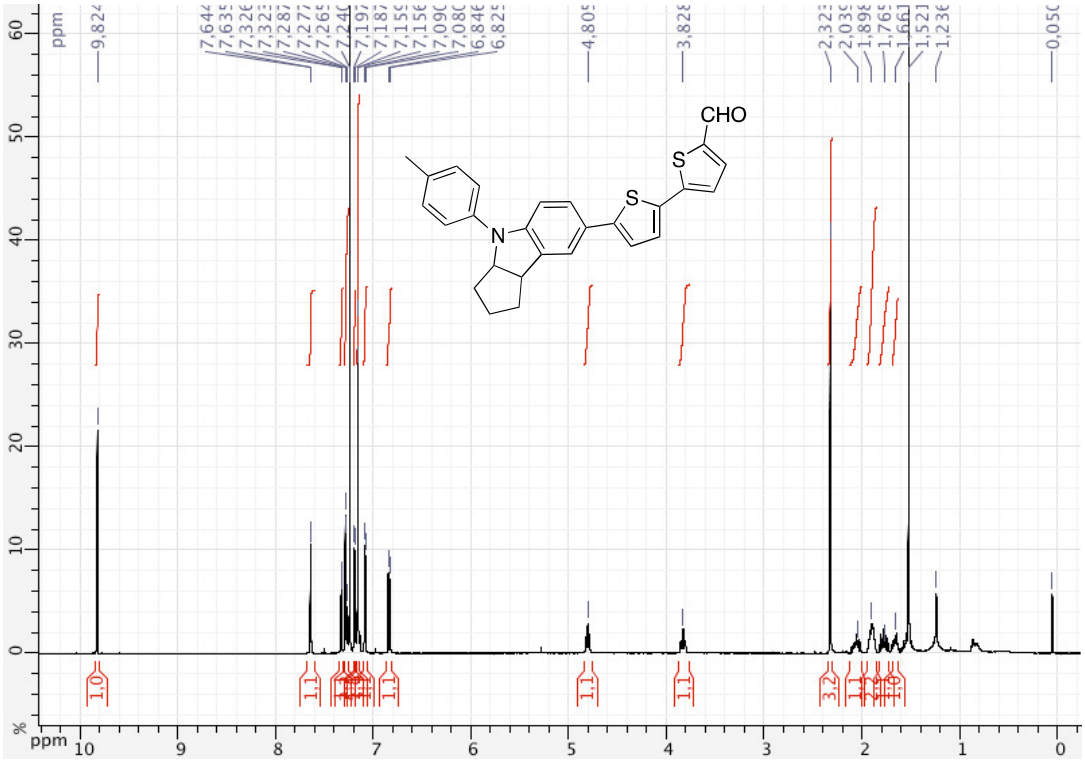

Fig. S1.4 ^{1}H NMR spectra of compound **6** (LC159) recorded in $CDCl_3$.

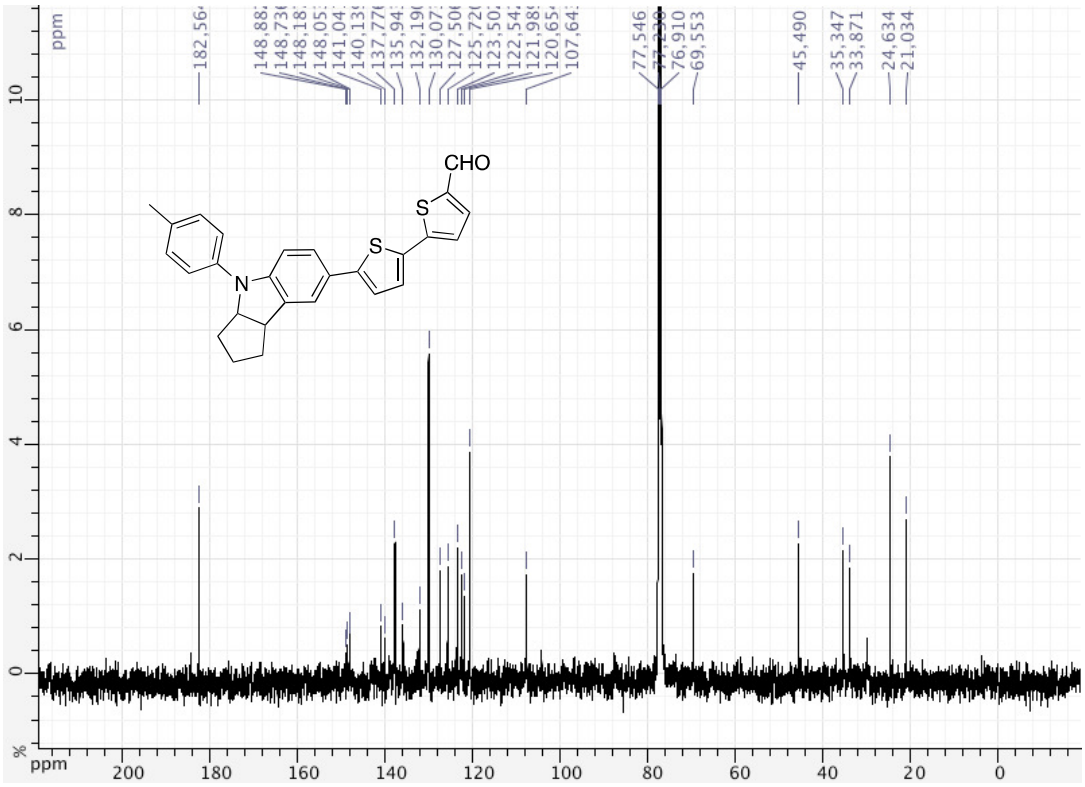

Fig. S1.5 ^{13}C NMR spectra of compound **6** (LC159) recorded in $CDCl_3$.

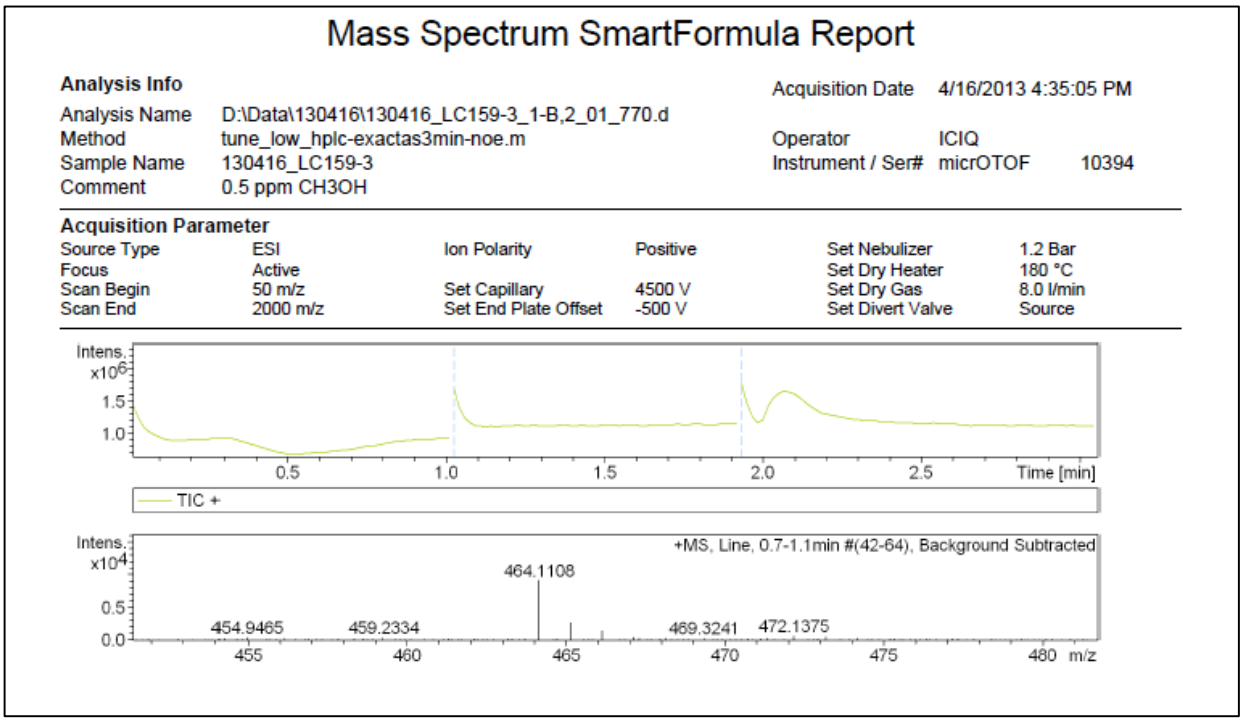

Fig. S1.6 HRMS (ESI) spectrum of compound **6** (LC159).

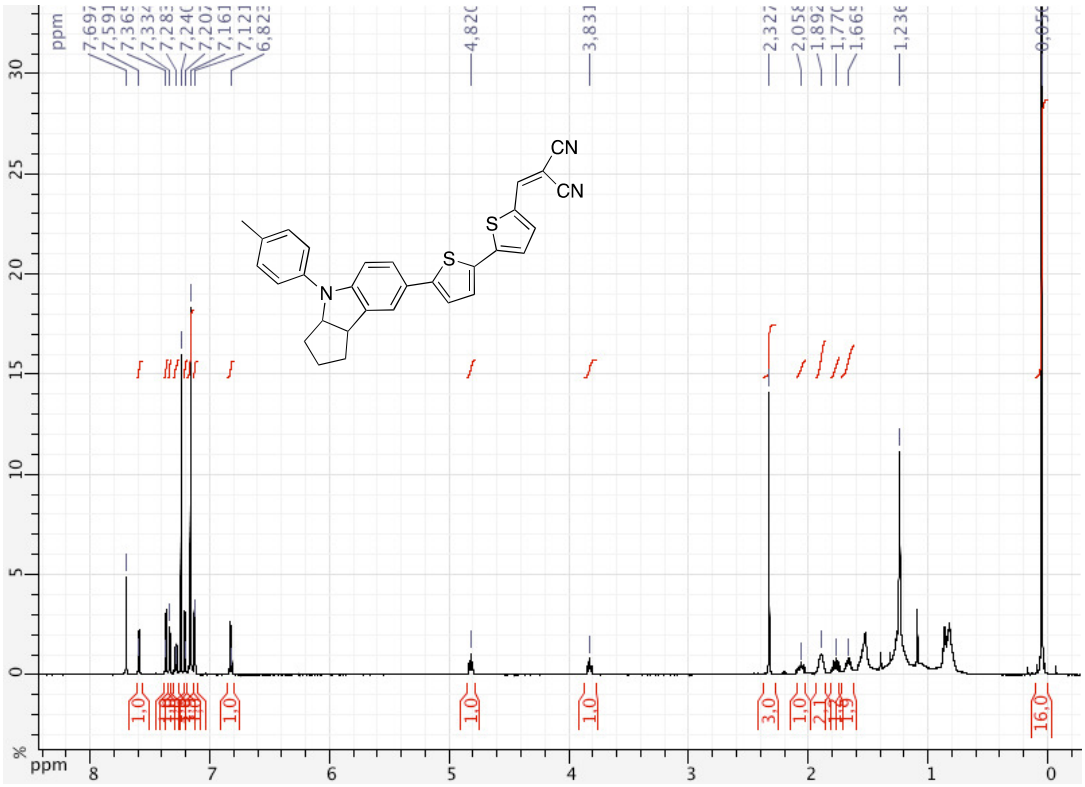

Fig. S1.7 ^{1}H NMR spectra of compound **LC163** recorded in $CDCl_3$.

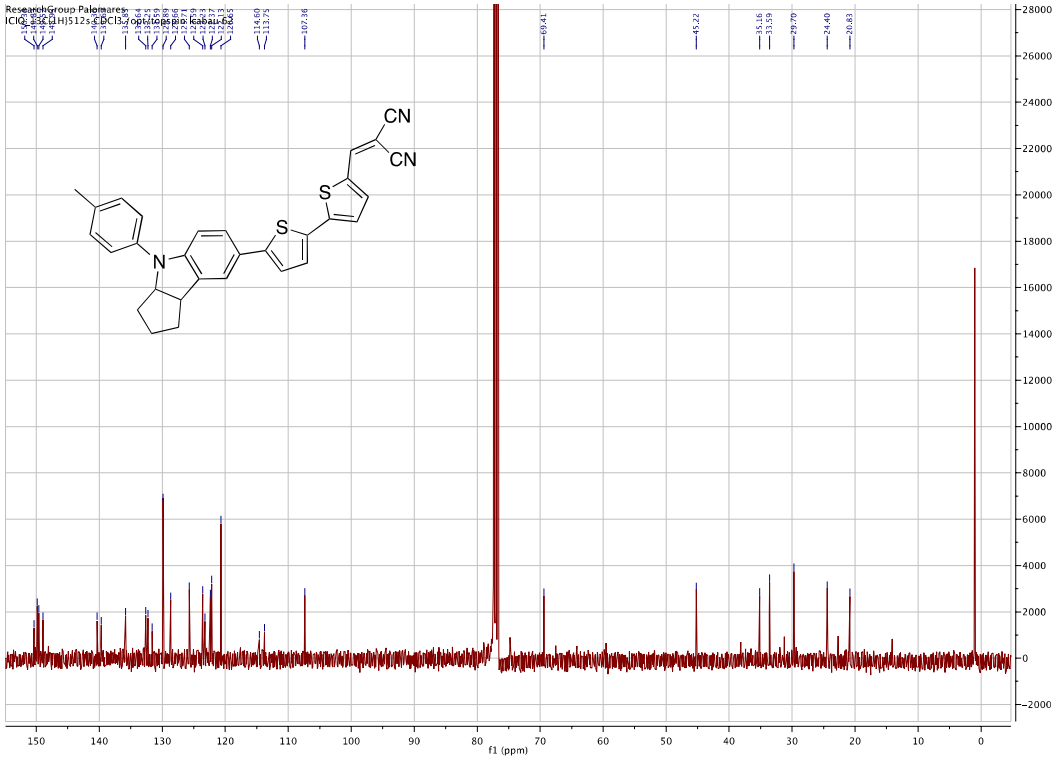

Fig. S1.8 ^{13}C NMR spectra of compound **LC163** recorded in $CDCl_3$.

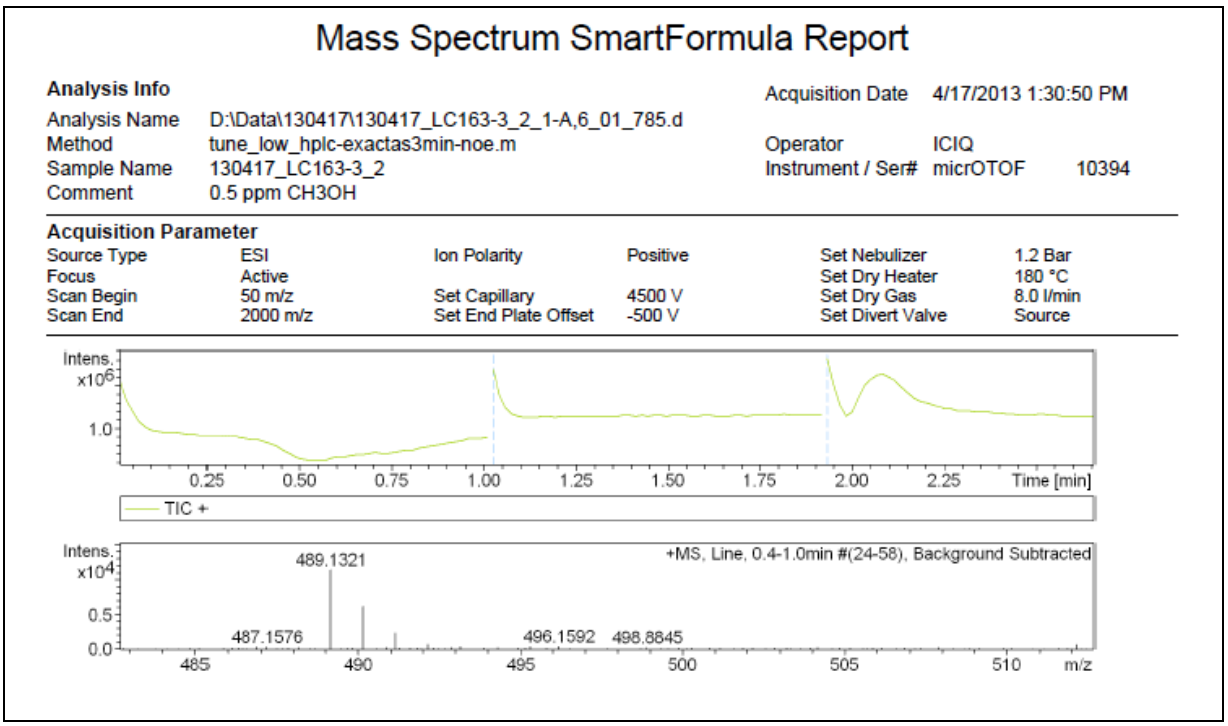

Fig. S1.9 HRMS (ESI) spectrum of compound **LC163**.

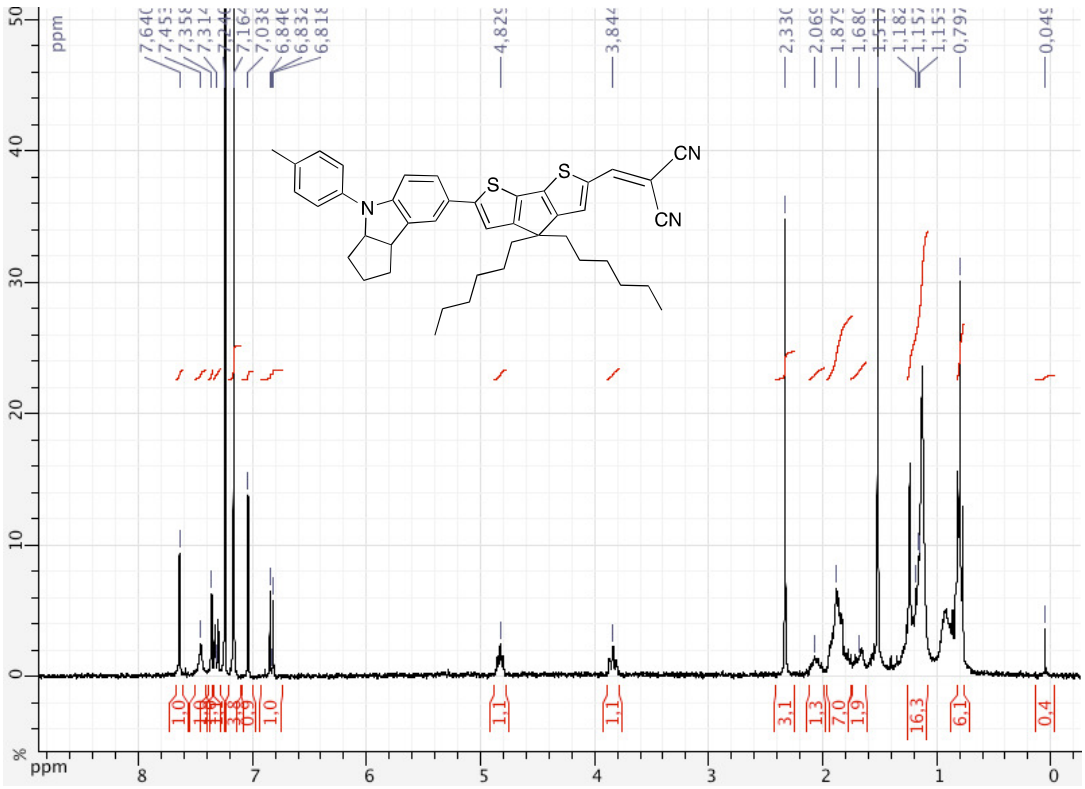

Fig. S1.10 ^{1}H NMR spectra of compound **VC63** recorded in $CDCl_3$.

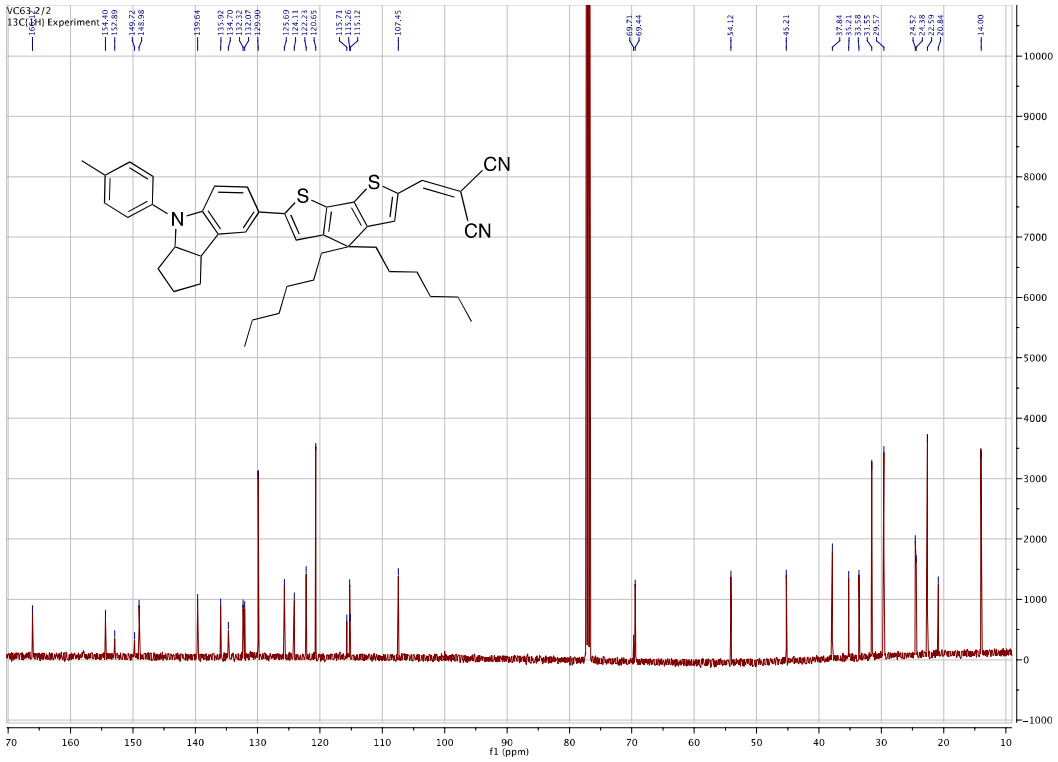

Fig. S1.11 ^{13}C NMR spectra of compound **VC63** recorded in $CDCl_3$.

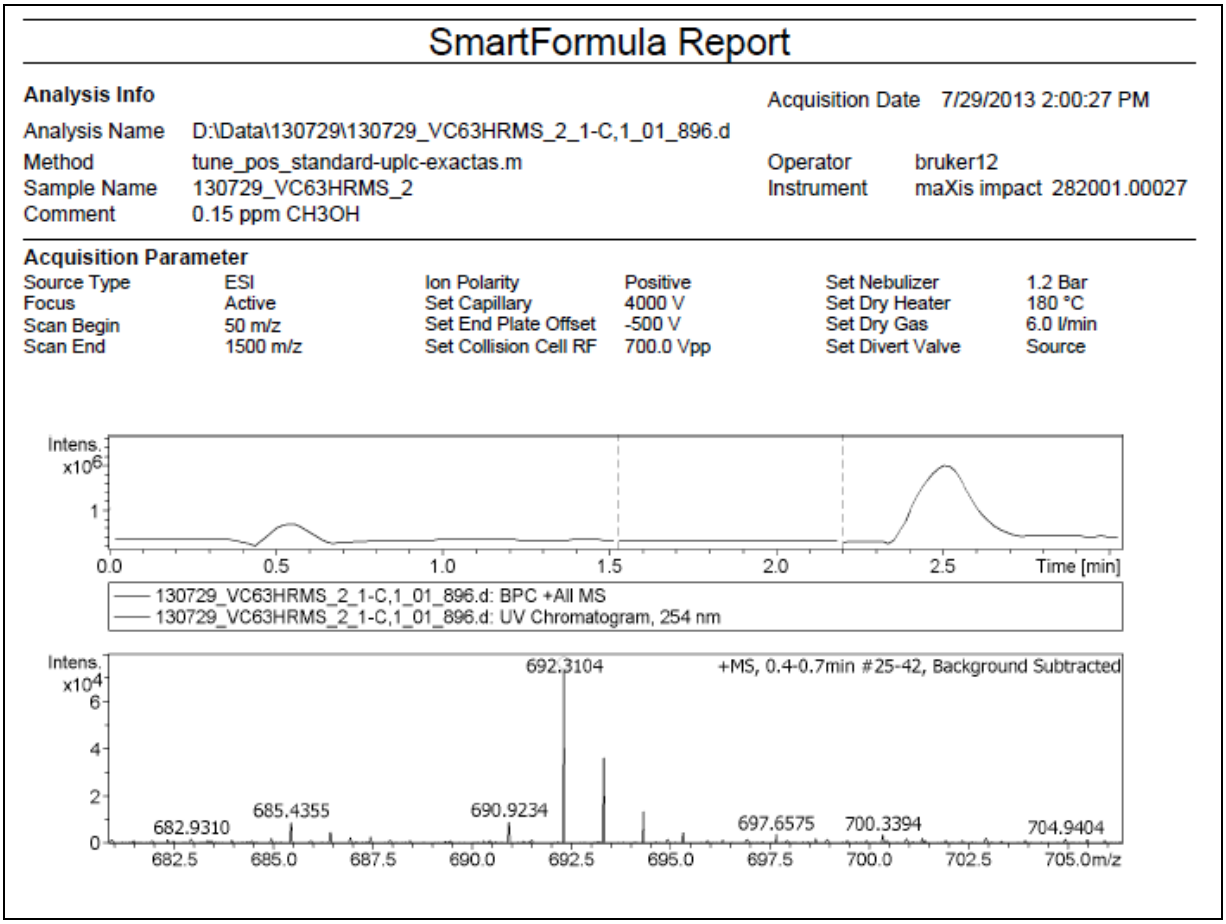

Fig. S1.12 HRMS (ESI) spectrum of compound **VC63**.

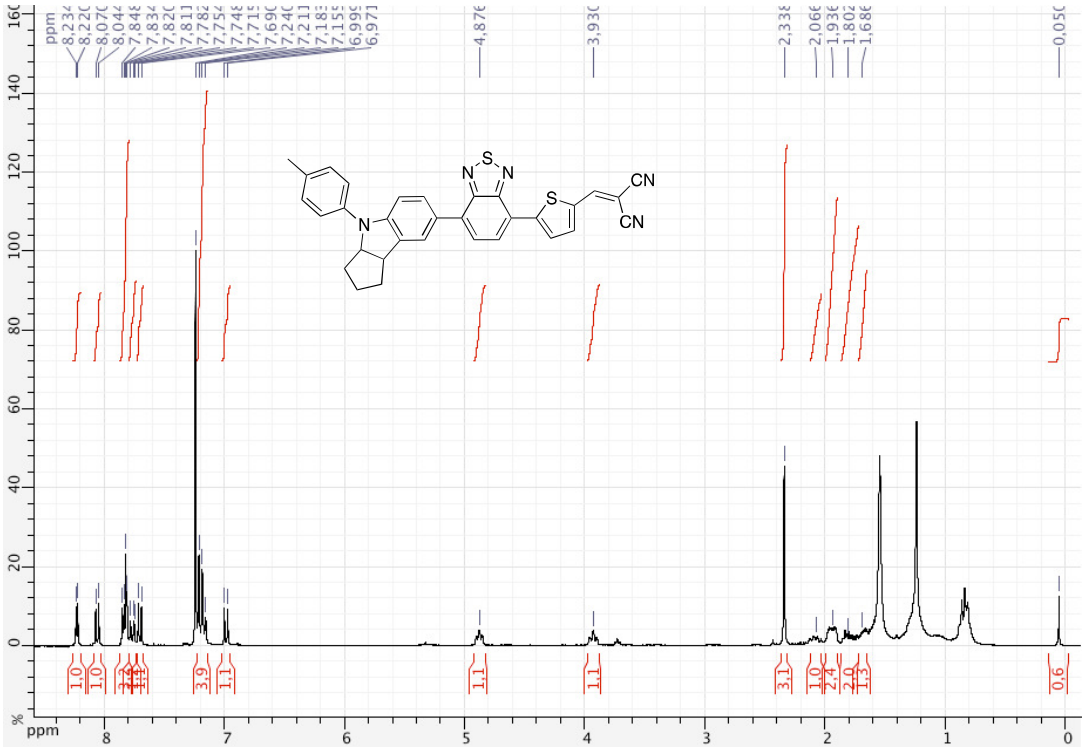

Fig. S1.13 ^{1}H NMR spectra of compound **VC64** recorded in $CDCl_3$.

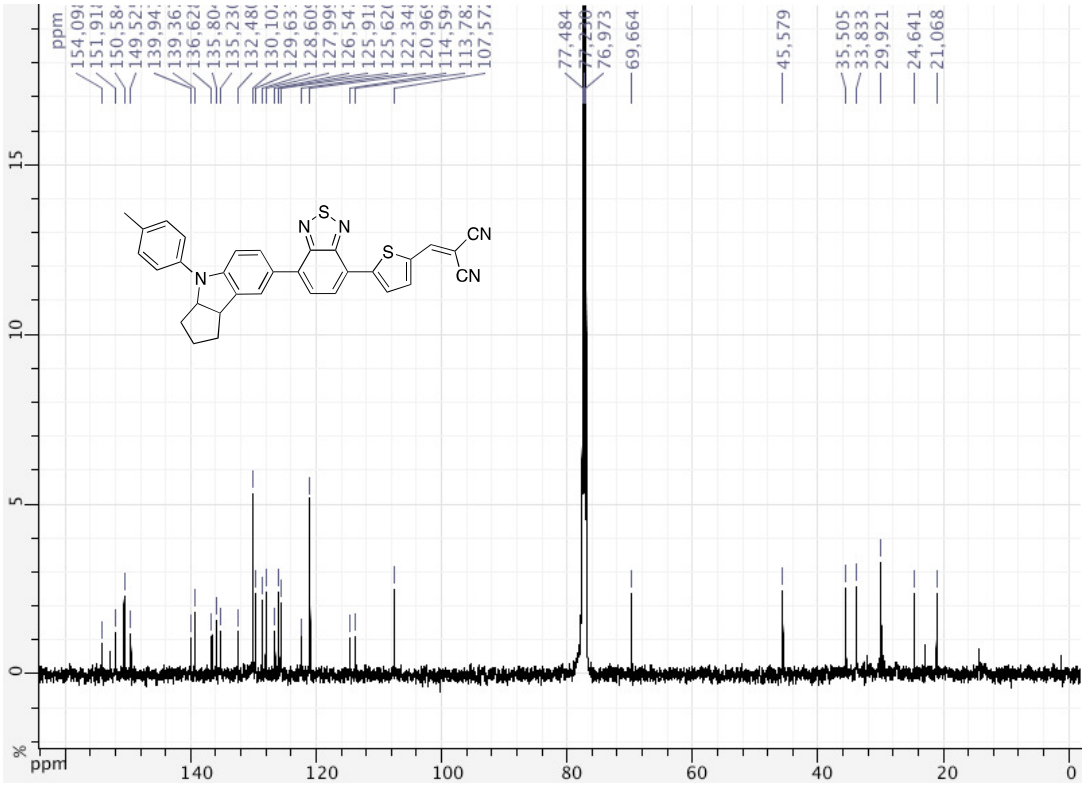

Fig. S1.14 ^{13}C NMR spectra of compound **VC64** recorded in $CDCl_3$.

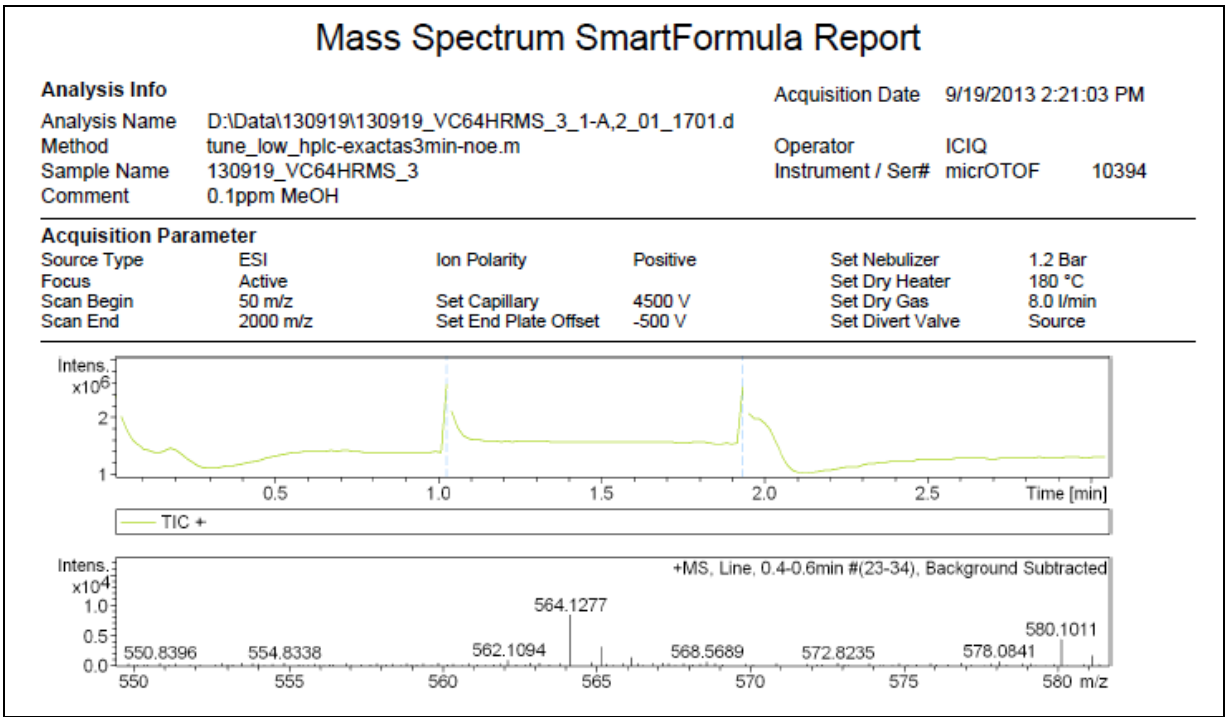

Fig. S1.15 HRMS (ESI) spectrum of compound **VC64**.

S2. Square wave voltammetry plot

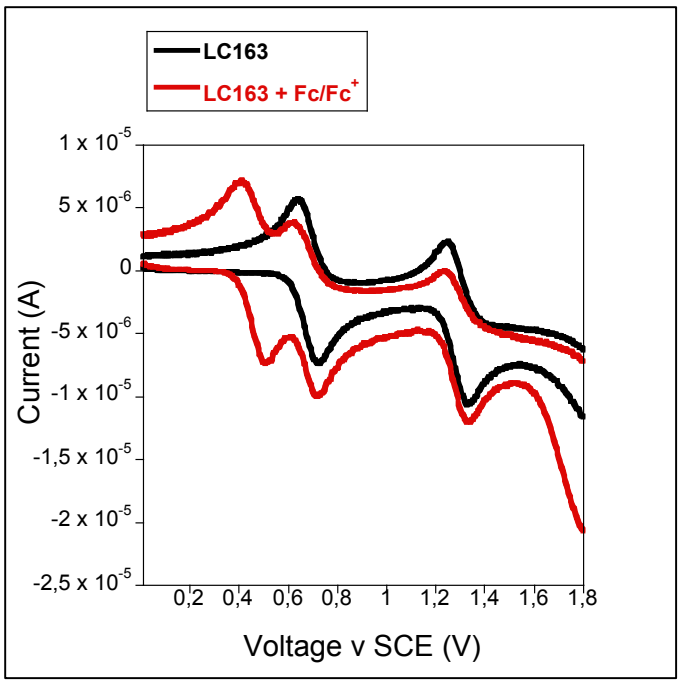

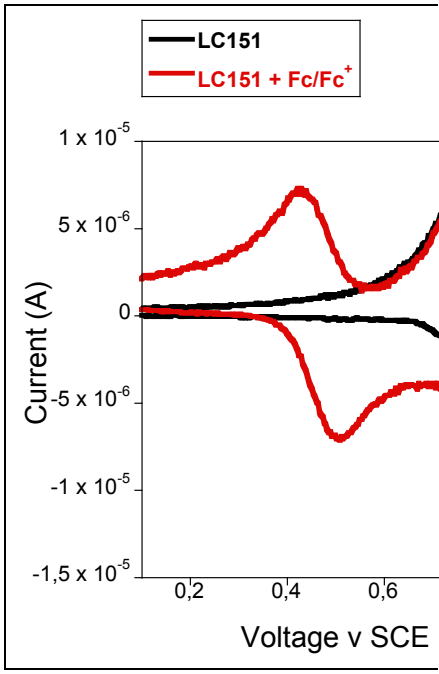

S2.1 Cyclic voltammetry of **LC151** and **LC163**.

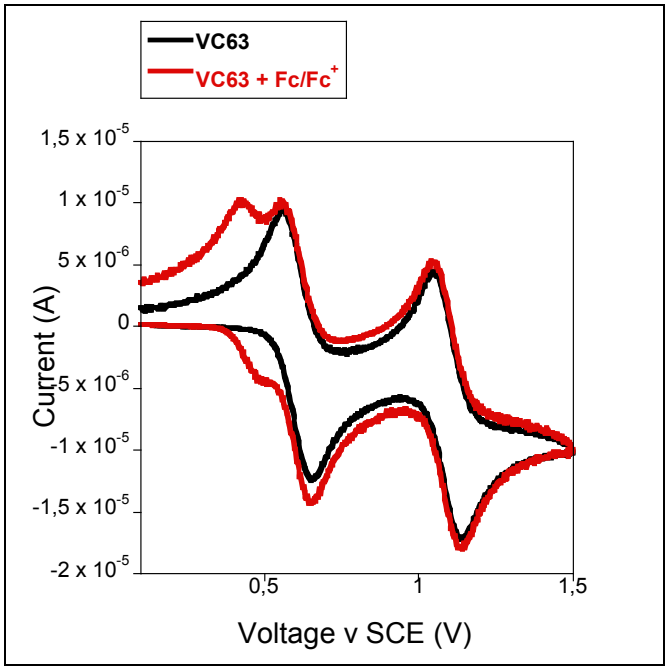

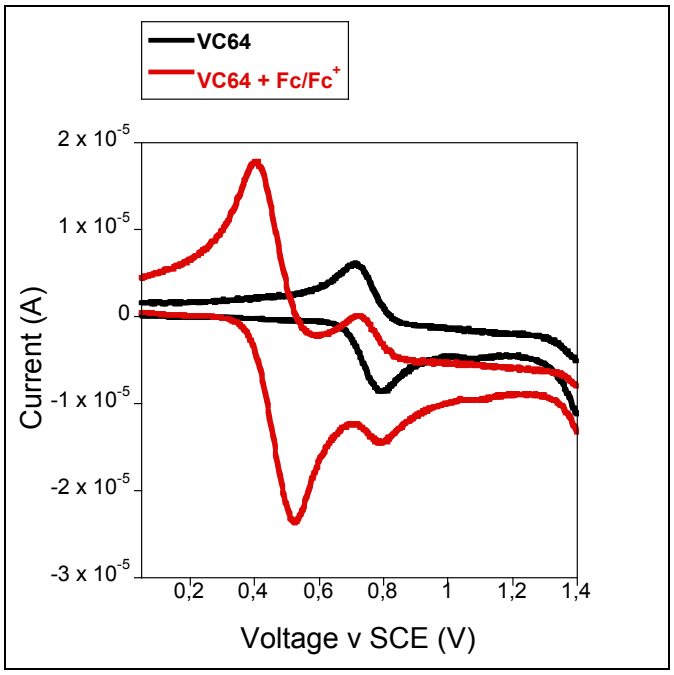

S2.2 Cyclic voltammetry of **VC63** and **VC64**.

CV Measurements All these CV were recorded by PARSTAT 2273 (Princeton Applied Research) in 0.1M tetrabutylammonium hexafluorophosphate in dichloromethane (DCM) at a scan rate of $30mVs^{-1}$. The working electrode consisted of a platinum wire and the counter electrode a platinum mesh. The reference electrode was the silver calomel electrode (saturated KCl). All solutions were degassed with argon for 5 minutes prior to measurement. The red and black scans were recorded in the presence and absence of Ferrocene/$Ferrocene^{+}$.

S3. UV-Visible and emission spectroscopies

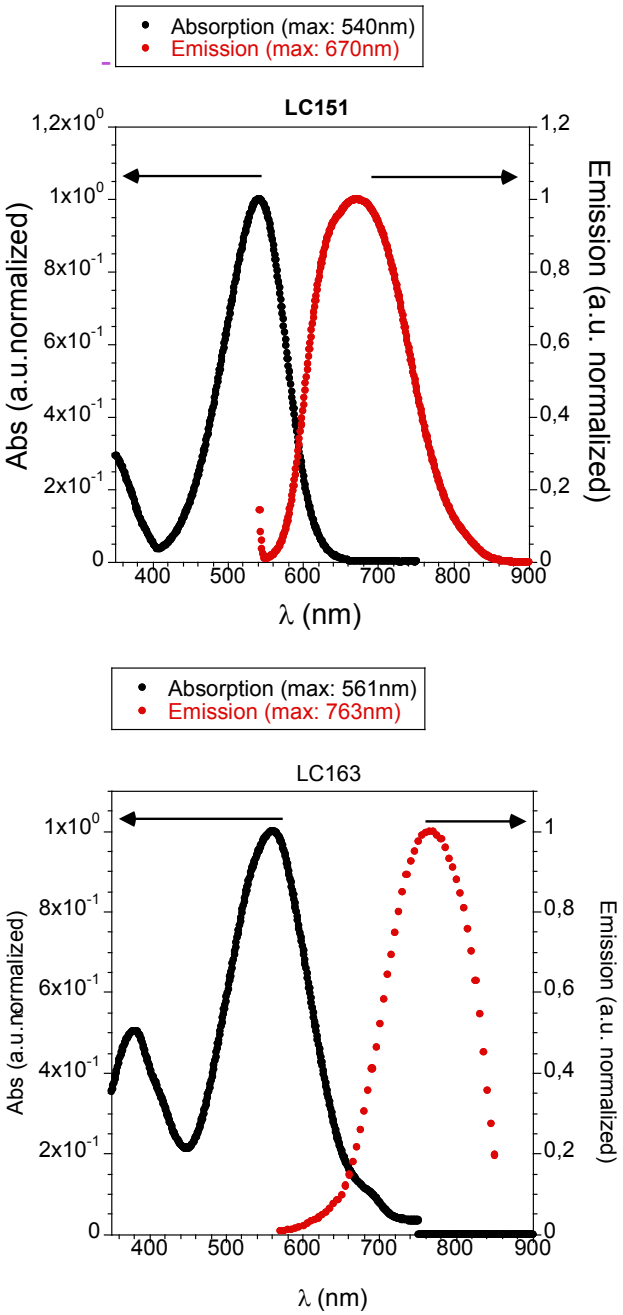

S3.1 Steady-state fluorescence emission measurements of **LC151** and **LC163**.

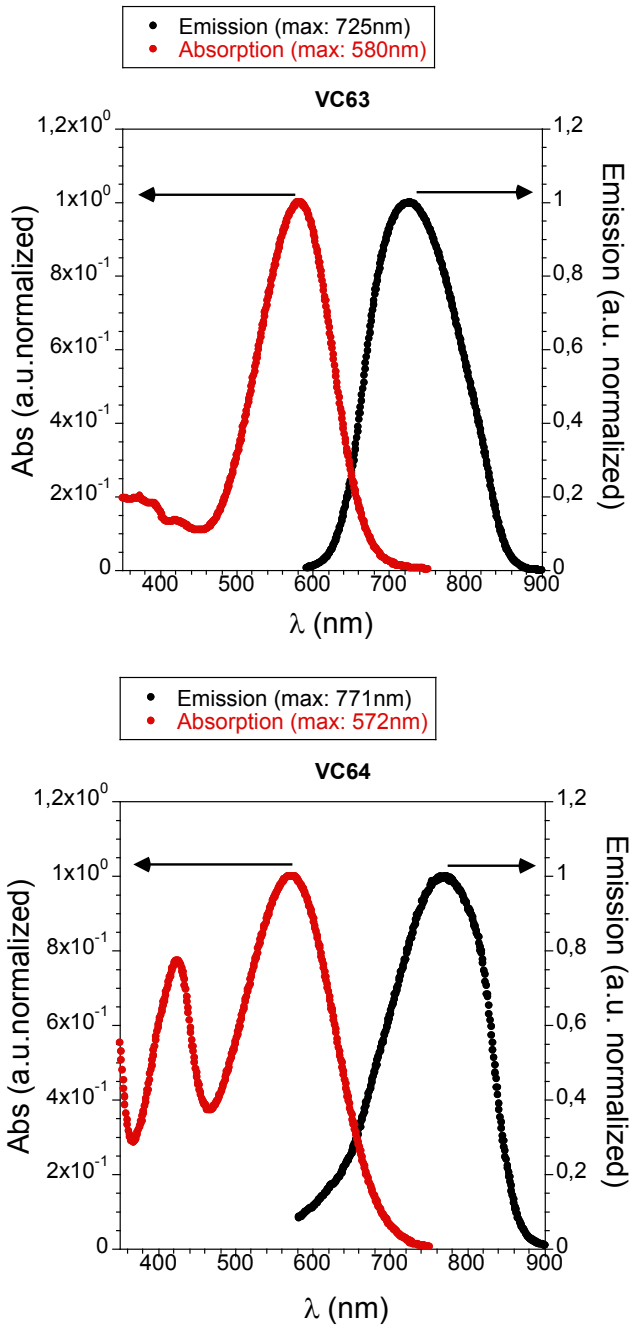

S3.2 Steady-state fluorescence emission measurements of **VC63** and **VC64**.

UV-Visible measurements. UV-Vis measurements were carried out on a Shimadzu UV 3600 spectrophotometer. For extinction coefficient determination, solutions of different concentration were prepared in CH_2Cl_2 (HPLC grade) with absorption between 0.1-1 of absorbance using a 1 cm UV cuvette. The emission measurements were carried out on Cary Eclipse fluorescence spectrophotometer.

Steady-state fluorescence emission measurements. The thin films emission properties were recorded using a Perkin-Elmer© fluorimeter with the appropriated holder for solid and film samples.

S4. Device optimization

Table S4.1. Device performance parameters of **LC151.**

w/w ratio	Thickness (nm)	Jsc (mA/cm2)	Voc (mV)	FF (%)	PCE (%)
1:1	57	5.62	934	46.09	2.42
	57 (non-A)	5.41	889	43.93	2.11
2:1	55	3.13	959	32.64	0.98
	55 (non-A)	3.48	934	32.81	1.07
1:2	55	7.48	915	45.24	3.09
	55 (non-A)	6.76	859	41.75	2.42
	42	6.75	925	46.88	2.92
	48	7.49	925	45.34	3.12
	57	7.67	920	46.15	3.26
	65	8.32	915	43.79	3.34
	86	7.75	915	41.45	2.94
	120	5.81	894	32.66	1.70
1:3	59	5.22	915	47.61	2.28
	59 (non-A)	4.53	890	46.02	1.86

Table S4.2. Device performance parameters of **LC163.**

w/w ratio	Thickness (nm)	Jsc (mA/cm2)	Voc (mV)	FF (%)	PCE (%)
1:1	68	4.47	774	41.45	1.43
	68 (non-A)	4.21	769	41.27	1.34
	45	4.10	764	43.59	1.37
1:2	62	5.43	753	41.88	1.72
	62 (non-A)	4.81	768	40.68	1.50
1:3	63	4.90	754	41.63	1.54
	63 (non-A)	4.51	754	39.08	1.34
	78	5.15	769	38.99	1.54

Table S4.3. Device performance parameters of **VC63.**

w/w ratio	Thickness (nm)	Jsc (mA/cm2)	Voc (mV)	FF (%)	PCE (%)
1:1	70	1.74	740	32.21	0.41
2:1	68	0.90	765	28.24	0.19
1:2	67	3.04	729	38.33	0.85
	67 (non-A)	2.91	734	37.83	0.81
1:3	60	2.92	699	31.43	0.64

Table S4.4. Device performance parameters of **VC64.**

w/w ratio	Thickness (nm)	Jsc (mA/cm2)	Voc (mV)	FF (%)	PCE (%)
1:1	59	4.80	859	40.76	1.68
	59 (non-A)	4.45	854	40.66	1.54
2:1	62	2.78	849	45.77	1.08
	62 (non-A)	2.60	854	43.81	0.97
1:2	65	6.42	864	43.98	2.45
	65 (non-A)	5.40	860	43.69	2.03
	81	5.81	769	39.76	1.78
1:3	66	3.29	849	27.14	0.76
	66 (non-A)	2.90	814	28.65	0.68

S5. AFM images

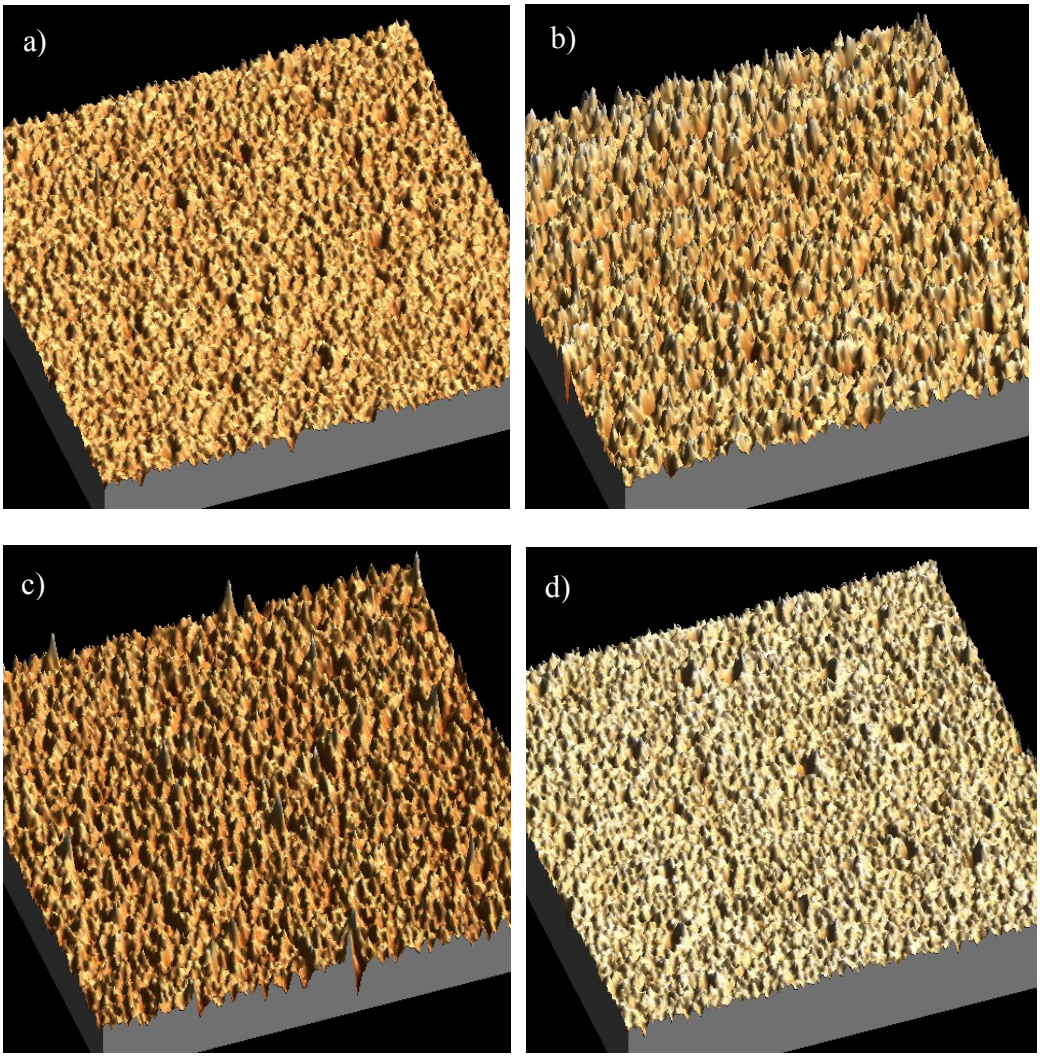

Figure S5.1. 3D AFM images of a) LC151:$PC_{70}BM$, b) LC163:$PC_{70}BM$, c) VC63:$PC_{70}BM$ and d) VC64:$PC_{70}BM$.

AFM images were taken in order to detect some variations that could correlate the differences between the devices (based on the four different

molecules), the images depicted more roughness for LC163 (b) and VC63 (c) compared to LC151 (a) and VC64 (d); however the difference observed is not determinant to find a direct correlation between the aggregates (the surface distribution) and the final device performance. We assume in this study that these nanomorphology variations include the individual molecule orientation and molecular packing.

S5. Mobility measurements

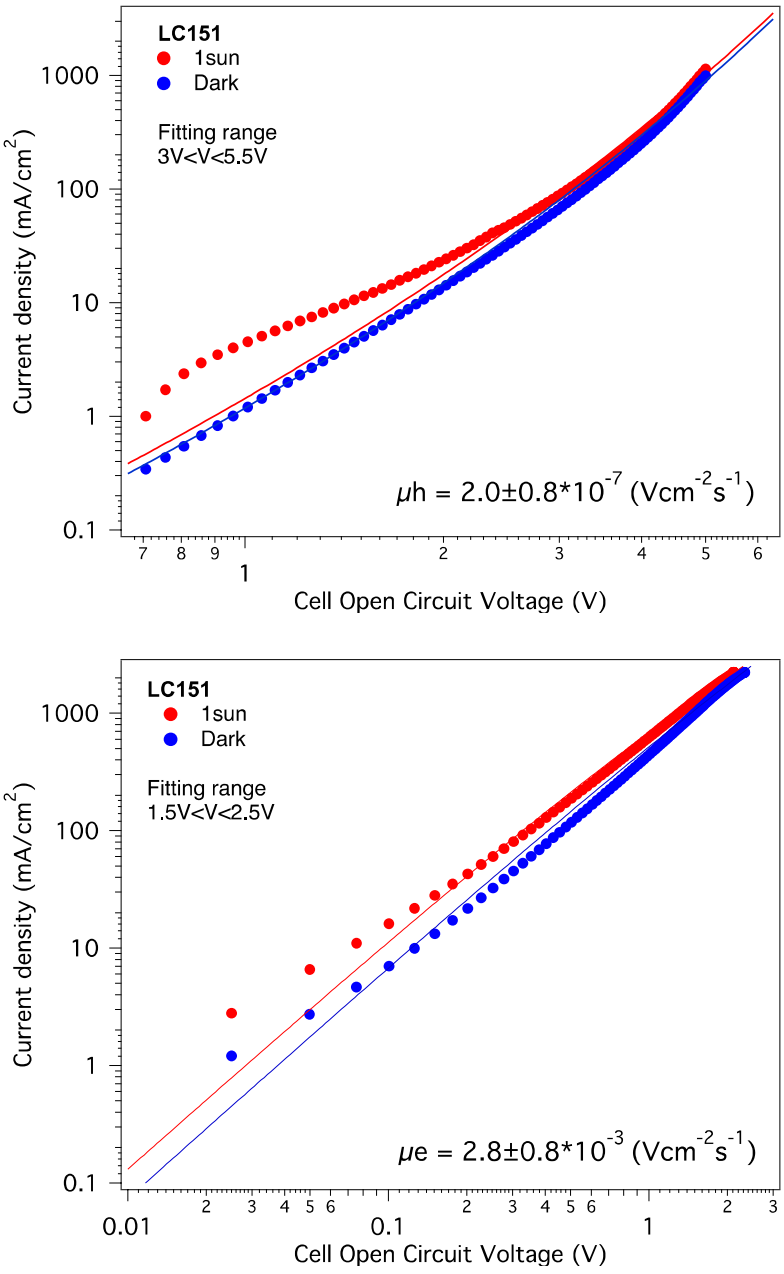

Figure S5.1. Hole only and electron only **LC151** devices J-V curves at space charge limited conditions.

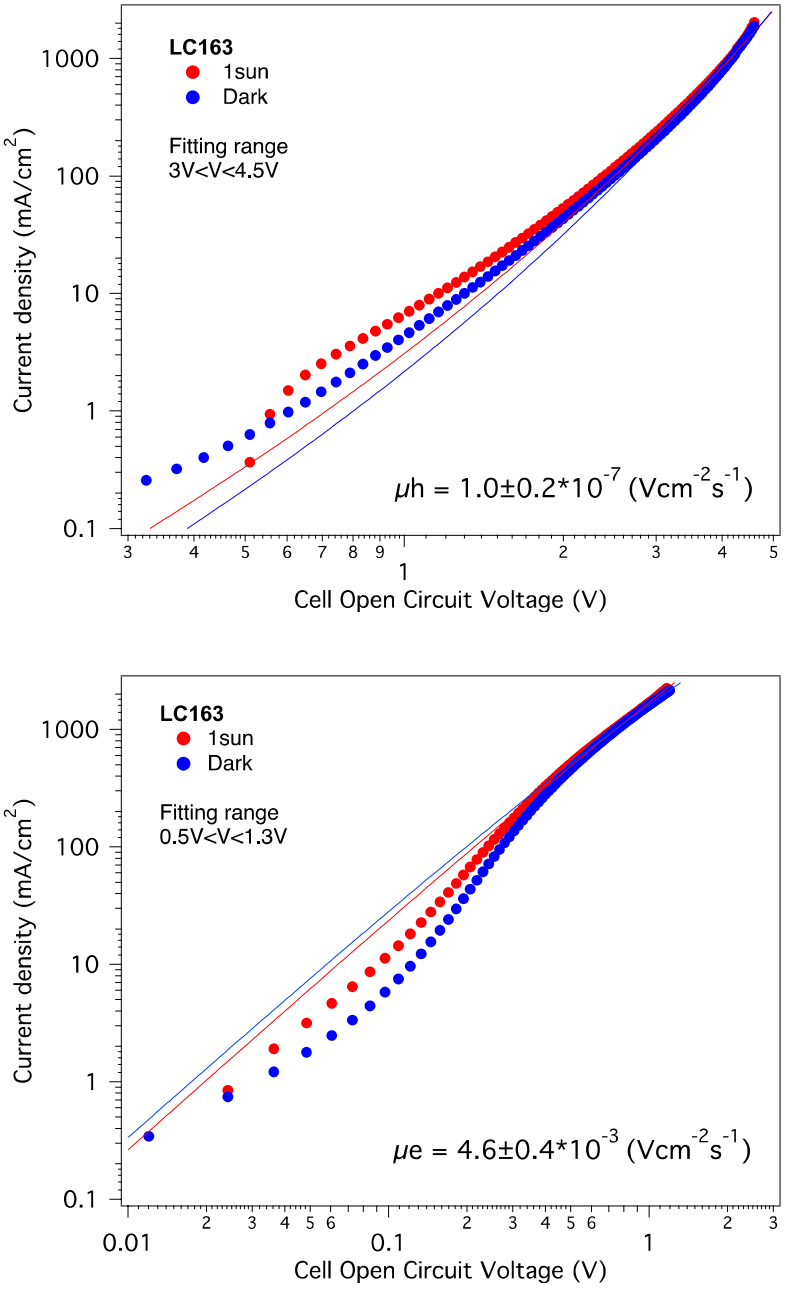

Figure S5.2. Hole only and electron only **LC163** devices J-V curves at space charge limited conditions.

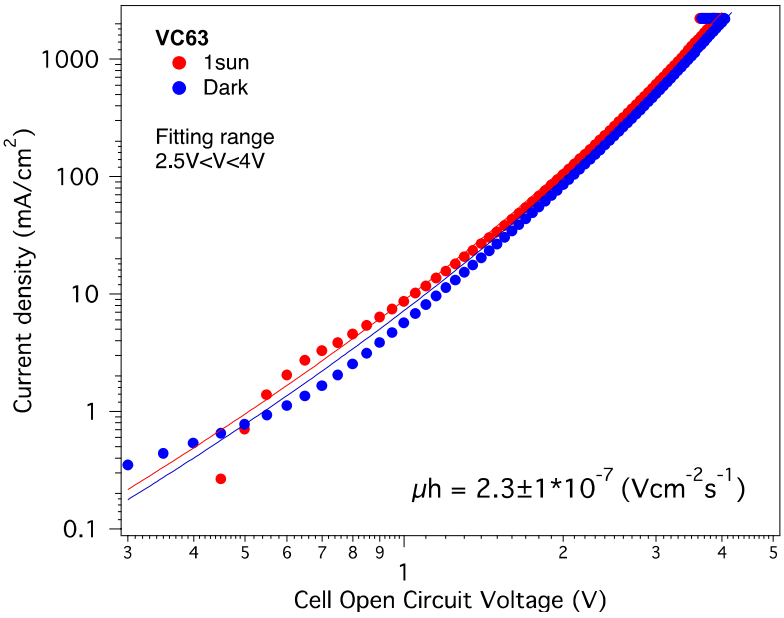
VC63
1sun
Dark
Fitting range
2.5V<V<4V
μh = 2.3±1*10^-7 (Vcm^-2s^-1)
Current density (mA/cm^2)
Cell Open Circuit Voltage (V)

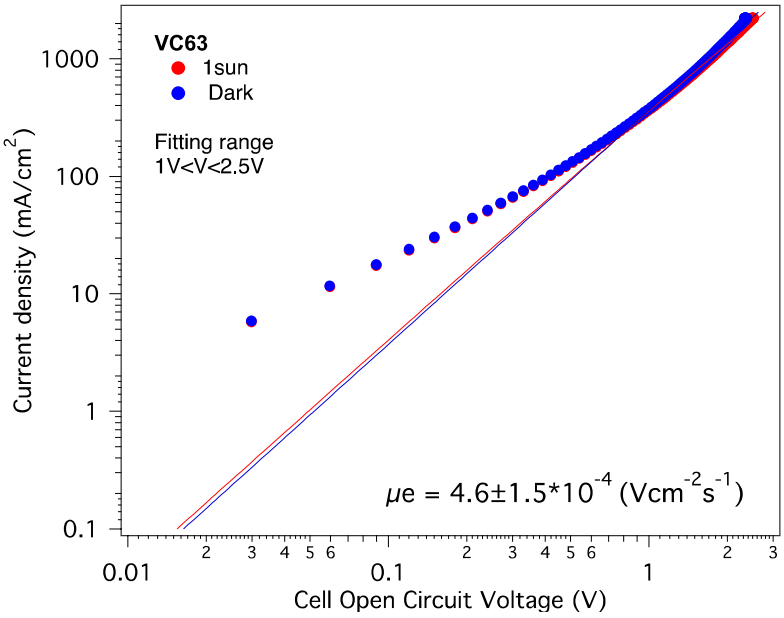
VC63
1sun
Dark
Fitting range
1V<V<2.5V
μe = 4.6±1.5*10^-4 (Vcm^-2s^-1)
Current density (mA/cm^2)
Cell Open Circuit Voltage (V)

Figure S5.3. Hole only and electron only **VC63** devices J-V curves at space charge limited conditions.

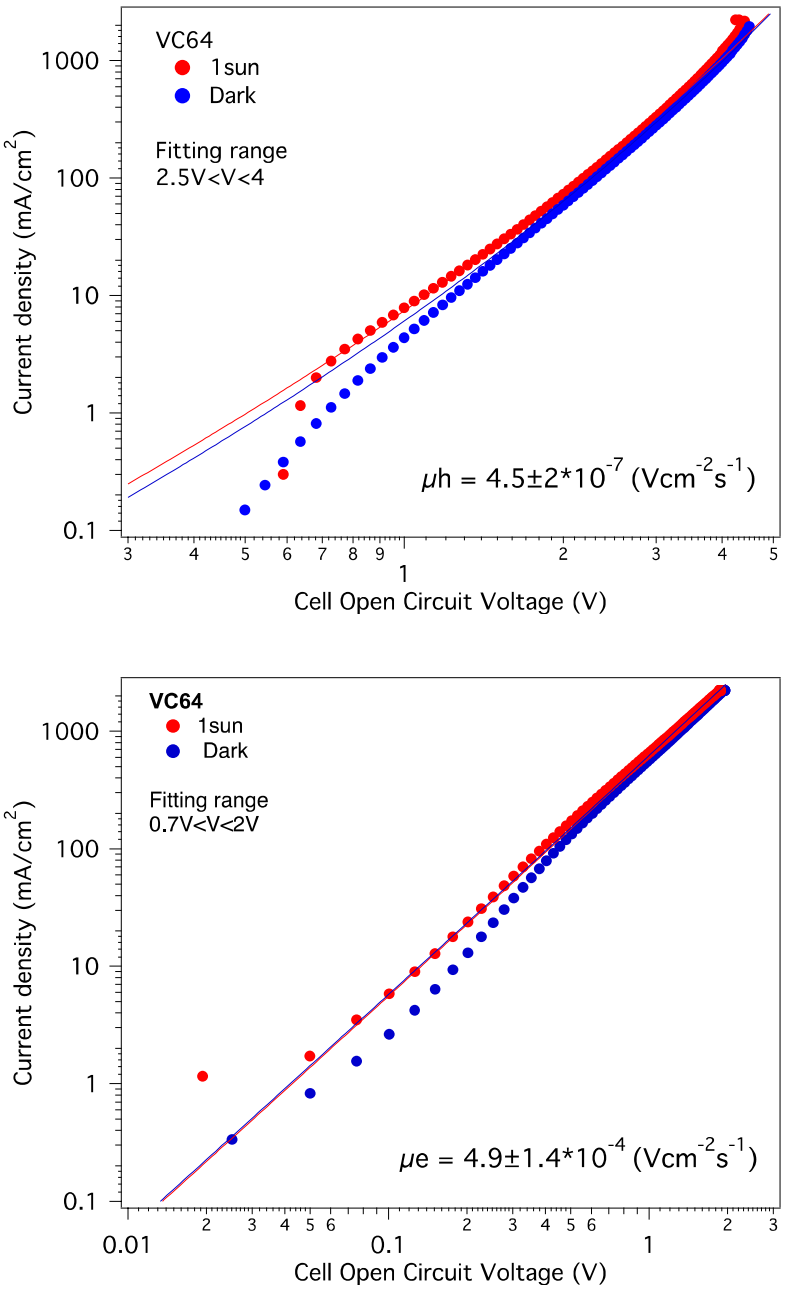

Figure S5.4. Hole only and electron only **VC64** devices J-V curves at space charge limited conditions.